Detection of changes in dynamic characteristics of composite structures using Kriging metamodelling procedure: Experimental and computational analysis

Kleison A. Possenti[1], Vanessa G. S. de Menezes[1], Dirk Vandepitte[2], Volnei Tita[3,4], Ricardo de Medeiros[1]

[1]*UDESC, Santa Catarina State University, Department of Mechanical Engineering, Rua Paulo Malschitzki, 200, 89.219-710, Joinville, Santa Catarina, Brazil*

[2]*KU Leuven, Department of Mechanical Engineering, Celestijnenlaan 300 box 2420, Heverlee, B-3001, Belgium*

[3]*EESC-USP, University of Sao Paulo, Sao Carlos School of Engineering, Department of Aeronautical Engineering, Av. João Dagnone, 1100, 13573-120, São Carlos, SP, Brazil*

[4]*FEUP, Faculty of Engineering of University of Porto Department of Mechanical Engineering, Rua Dr. Roberto Frias, s/n, 4200-465, Porto, Portugal*

Abstract

To ensure the quality, safety, and long-term durability of fiber-reinforced composite components, it is necessary to explore approaches for monitoring and detecting defects or damage. Non-destructive detection techniques based on dynamic properties and structural response, such as natural frequency, damping, and modal shape. This study presents a numerical-experimental methodology based on dynamic analysis of structures made of composite materials. The methodology utilizes a surrogate model to establish a design envelope through a Kriging metamodel and to assess a damage index for structures affected by impact damage. The Latin Hypercube method is employed to generate values for the input variables, while the Finite Element Method (FEM) is utilized to calculate the natural frequencies. The Kriging metamodel is then employed to generate a numerical model, which is optimized using the Efficient Global Optimization (EGO) algorithm and the Expected Improvement metric (EI) to minimize computational costs. The methodology yields a frequency range and determines a design envelope to evaluate the manufacturing quality of the structure. A damage index is used to identify structures with defects or impact damage, allowing for the assessment of severity. Additionally, the study evaluates the impact of incorporating metrics into the Latin Hypercube method to further reduce computational costs. Finally, this proposed approach contributes to the development of monitoring systems for assessing the manufacturing quality of composite structures and detecting impact damage through dynamic analysis. By utilizing this methodology, it becomes possible to effectively identify and evaluate the severity of defects and damage in composite structures, thus enhancing quality evaluation processes.

Keywords: Low-frequency Dynamics, Composite Plates, Manufacturing Defects, Finite Element Analysis, Design of Experiments.

1. Introduction

With the advancement of technological development, more complex structures require specific materials [1-2]. The combination of low weight, high strength, high stiffness, and resistance to abrasion and impact is difficult to find in conventional materials [3-4]. Composite materials provide new opportunities for high-performance structures. By combining two or more different materials, structural properties are different from the properties of each of the components [5]. However, unlike metallic structures, composite properties are not easy to control during the manufacturing, and as a consequence, some level of uncertainty in the properties of these materials is usually inevitable. These uncertainties make the design task difficult and increase the probability of errors in predicting the structural life cycle. Strict control and monitoring of the loss of structural properties is required to prevent a premature failure of the structure. These losses can occur due to the low quality of the manufacturing process, and damage suffered during their lifetime by external agents. The development of efficient methodologies and monitoring systems for detecting defects and/or damage in composite structures is important to avoid catastrophic failure [6-9]. According to [1], damage and defects can occur during materials processing, component manufacture, or in-service use. The present work considers defects which originate from the manufacturing process, and damage is caused due to the in-service use, such as an impact event.

Vibration characteristics of the structure qualify as an indicator for detecting and monitoring defects and damage in composite structures. Vibration-based damage methods (VBM) follow the changes in the dynamic structural response caused by the defect or the damage. These changes are sensed by structural health monitoring (SHM) system, which then compare the responses of intact and damaged structures in terms of mode shapes, natural frequencies, or damping factors using damage indices. The SHM system estimates the severity of defect or damage and it can make a prognosis of the structure in terms of service life [10]. Dynamic analyses show high potential not only to be applied in SHM systems but also to be used as Non-Destructive Test [11-12]. the Frequency Response Functions (FRF) provide a very adequate metric for this task in composite structures [13]. Several damage detection methods assume that damage causes changes in the mass and/or stiffness of the structure [14-16], which naturally change the FRF. However, to guarantee that the change in the FRF is caused by damage which originates from in-service usage, non-destructive testing on the structure is required before it is put in service to verify the presence of manufacturing defects [17-19]. This task is particularly relevant for composite structures, where the manufacturing process has a high number of parameters to be controlled.

To address complex problems with a large number of parameters, Finite Element Analysis (FEA) can be a useful approach. FEA is particularly effective in tackling structural optimization problems, which have gained significant attention, especially when combined with the study of structural reliability. By utilizing FEA, engineers and researchers can create models of physical structures and analyze how they behave under different conditions, allowing them to optimize designs and improve the reliability of structures [20]. However, these problems have a high computational cost due to the large numbers of numerical models that must be solved, taking into account the range of parameter settings and parameter combinations that are required. Many techniques used in regression analysis and prediction modeling, such as kriging [20-28], multivariate adaptive regression splines (MARS) [29-30], and response surface [31-32]. Choosing the appropriate method depends on the nature of the data, the problem at hand, and the goals of the analysis. For example, kriging is more suitable for spatial data, especially when spatial autocorrelation is present, while response surface modeling and MARS are better suited for simpler datasets with a focus on non-spatial relationships and interpretability.

In this context, the concept of surrogate models is useful in this respect, such as the Kriging metamodel, which has been used in optimization problems. In addition, due to the high computational cost of the objective function, Efficient Global Optimization (EGO) can be used, which is efficient to limit the number of evaluations of the objective function [21-23]. Literature provides scientific contributions that surrogate models that are specifically developed for composite structural analysis. Echaabi *et al.* [24] present a review of different failure criteria (Tsai-Wu, maximum stress and strain, Hashin criterion, and Hart-Smith criterion) with a Kriging metamodel. The authors discuss the computational implementation, pointing out the validity, advantages, and limitations of each case. Lanzi and Giavotto [25] propose a multi-objective optimization procedure for the design of composite stiffened panels in post-buckling states. The procedure is based on genetic algorithms with three different methods of global optimization: neural networks, radial basis functions, and Kriging approximation. Their results prove that the initial imperfections (defects) affect not only the first-buckling load but also the post-buckling range up to collapse. Jansson *et al.* [20] evaluate approximation models used in conjunction with genetic algorithms via a generic beam structure as an example problem. The accuracy of four different approximation methods is assessed, polynomial models with and without term selection, radial basis functions, and Kriging. Lu *et al.* [26] propose an inverse procedure to identify the mechanical properties of both the carbon fibre and the interphase region based on computational micromechanics with a Kriging metamodel. Mukhopadhyay *et al.* [27] show a critical comparative assessment of Kriging model variants for surrogate-based

uncertainty propagation considering stochastic natural frequencies of composite doubly-curved shells. The study reveals that universal Kriging coupled with marginal likelihood estimate yields the most accurate results, followed by Co-Kriging and Blind Kriging. Pavlack *et al.* [28] investigate the performance of a data-driven methodology for quantifying damage based on the use of a metamodel obtained from a Polynomial Chaos Kriging method. Polynomial Chaos Kriging shows promising results for capturing the proper trend for the severity of the damage as a function of the damage index.

The present work consists of an additional contribution to a methodology, which has been developed by the authors over the years [17-18, 33-38]. The proposed procedure goals to detect and monitor defects from the manufacturing process as well as damage from in-service usage of composite structures, such as impact events. In a first step, design variables are investigated that are most affected by the manufacturing process. In other words, the variables are identified that have the strongest effect on the dynamic behaviour of the structure, defining the tolerance limits for a set of composite plates. In a second step, the finite element model is updated using the Kriging metamodel. Third, composite specimens are manufactured. This work uses a glass fibre and epoxy resin stack-up with sixteen layers, and two different types of reinforcements: unidirectional (UD) and bidirectional (BD). Physical vibration tests are carried out with the specimens. Results of both physical and virtual experiments are used to provide a range of possibilities for the FRFs, which can be applied to monitor and detect defects and damages based on damage indices. Finally, there is a discussion on defect and damage detection via VBM and metamodels.

2. Fundaments of Metamodels

Manufacturing defects are extremely complex to analyse, requiring enormous computational time, which hampers the optimization process. The alternative is the use of surrogate models (metamodels). It reduces the number of accesses to the objective function and, consequently, the computational time and resources, which are not always available. Thus, a metamodel consists of the approximation of a high-fidelity model that can be used to replace the original one. The construction of the surrogate model is based on obtaining an explicit function of low-cost $\hat{f}$ that the response is close to the response of the original model, which is called high fidelity. Thus,

$$f(x) = \hat{f}(x) + \varepsilon(x), \tag{1}$$

where $f(x)$ represents the response of the model to a certain point in the design space, $\hat{f}(x)$ is the response of the metamodel to this same point, and $\varepsilon(x)$ corresponds to the error.

In general, metamodels are applied to create models that are closer to reality. This modelling via response surface or metamodel is used to determine the minimum global. These metamodels are created by a curve or surface adjustment from a set of initial points based on a DoE (Design of Experiments), belonging to the search domain of the project variables [39]. In other words, the metamodel functions as an "interpolator curve" of the initial points without using the objective function. To build it, it is not necessary for the region where the minimum global [40]. So, this method is often used to replace the objective function to obtain a fast response. The response surface, once obtained, will be many orders of magnitude faster than a primary source, and still useful for predicting other function points [21].

2.1. Latin Hypercube

For sampling uniformly a design space, a rectangular grid of points can be used. Thus, Latin Hypercube (LH) designs have become particularly popular among strategies for computer experiments because it is an attractive sampling technique. It is flexible enough to provide data besides being capable of covering small to large design spaces. Point locations are determined using a random procedure [41]. To obtain an accurate model, the sampled points must be distributed as evenly as possible, filling the entire design space. An experiment design meets this characteristic by filling the space [21].

According to Forrester *et al.* [21], a Latin Hypercube can be constructed by splitting the design space into equal-sized bins and placing points in the bins, ensuring that in each bin, there is a unique point. Therefore, an experimental design can be written as p points and d dimensions into a matrix $p \times d$, where the column matrix represents the variables, and the row matrix represents the samples. A Latin Hypercube Sampling (LHS) is generated considering that each one of the d dimensions is divided into p equal levels, and there is only one point (or sample) in each level, aiming to generate points whose projections are orthogonal. Point locations are determined by a random procedure [41]. The maximin metric is one type of metric that can be used. Given the distances between the pairs of points present in the Latin Hypercube, position them in ascending order $\{d_1, d_2, \dots, d_n \,/\, d_1 < d_2 \,, \dots, d_{n-1} < d_n\}$ and try to maximize the shortest distance between the points, *i.e.,* d_1. After that, the procedure is repeated for the

distance d_2. In addition, in order to minimize J_j , *i.e*, to minimize the number of times a given distance d_j is repeated [42]. Distance setting can be set as

$$d_p\left(\boldsymbol{x}^{(1)}, \boldsymbol{x}^{(2)}\right) = \left(\sum_{j=1}^{k}\left|x_j^{(1)} - x_j^{(2)}\right|^p\right)^{\frac{1}{p}}, \tag{2}$$

where the index *i* represents the planes, *k* the dimension of the problem and *p* the norm used. For $p = 1$, it has the rectangular distance (Manhattan norm) and $p = 2$ the Euclidean norm. The use of the scalar value criterion function allows using these vectors and determining the best plane through the obtained index. Competing sampling plans can be classified through [43],

$$\Phi_q(\boldsymbol{X}) = \left(\sum_{j=1}^{m} J_j d_j^{-q}\right)^{\frac{1}{q}}, \tag{3}$$

where the smaller the value obtained for Φ, the better the sample space of *X*. Morris and Mitchell [43] suggested using values for *q* equal to 1, 2, 5, 10, 20, 50 and 100 and finding the best plan obtained between them through the maximin metric.

2.2. Kriging Metamodel

Metamodels are known as response surfaces, surrogates, emulators, and auxiliary models. According to Kleijnen *et al.* [23], a metamodel is an approximation of the input/output (I/O) function that is implied by the underlying simulation model. Surrogate models, such as Kriging, are fitted to data that are obtained for larger experimental areas.

Kriging model is constructed based on the correlation function theory. Particularly, it is an exact interpolation of the given data and goes through all the sampling points. Therefore, the Kriging model usually has a higher approximation accuracy than the traditional Root Mean Square (RSM). The Kriging model drastically reduces the computational time required for objective function evaluation in the optimization (optimum searching) process. This technique considers the relationship between input and output as a black-box system, and other system information, such as the internal process of dynamic analysis is not required. It can create, for example, a fast-running surrogate model to replace the exact Finite Element Analyses, and then the solving time of optimization will be reduced significantly. Thus, the potential of metamodel

techniques is indisputable in the model updating the field. A comparison of the most commonly used metamodels is presented by Simpson *et al.* [44].

The best linear unbiased predictor is a surrogate model, frequently used to represent a physical phenomenon or process, which is difficult to represent by numerical models or to measure experimentally. Kriging is considered a flexible model that depends on a set of parameters that control the properties of the model [45]. The goal of Kriging is to estimate the parameters that describe how the function typically behaves [46]. In this model, errors in predictions are considered dependent.

The building of the Kriging model starts with a given set of sample data, $\boldsymbol{X} = \{\boldsymbol{x}_1, \boldsymbol{x}_2, \ldots, \boldsymbol{x}_n^T\}$. Considering the responses $\boldsymbol{Y} = \boldsymbol{y}_1, \boldsymbol{y}_2, \ldots, \boldsymbol{y}_n^T$, the expression of the Kriging model reflects the relationship between them as

$$y(\boldsymbol{x}_i) = \boldsymbol{f}^T(\boldsymbol{x}_i)\boldsymbol{\beta} + z(\boldsymbol{x}_i), \tag{4}$$

where $\boldsymbol{f}^T(\boldsymbol{x}_i)$ is a polynomial vector of the sample $\boldsymbol{x}_i$, $\boldsymbol{\beta}$ is the vector of the linear regression coefficients to be estimated, and $z(\boldsymbol{x}_i)$ represents error and is assumed to be a stochastic process that follows a normal distribution of $N(0, \boldsymbol{\sigma}^2)$, with a zero mean and standard deviation $\boldsymbol{\sigma}$.

The fundamental assumption of the Kriging model is that the same input will lead to an identical output. Therefore, the deviation between the output response and the polynomial regression part is only due to the modelling error itself, regardless of the measurement error and other random factors. This method does not depend on the simulated precision of the polynomial part to the response surface but focuses on constructing the appropriate surrogate model by the effective filling of the stochastic process part, which makes it more suitable for dealing with non-linearity. Thus, the polynomial part is often taken as a constant in some other references.

To estimate the stochastic process $z(\boldsymbol{x}_i)$, the Kriging method assumes that the true response surface is continuous, any two points will tend to have the same value as the distance in between approaches zero, and it is the same for $z(\boldsymbol{x}_i)$ of two points. Thus, the correlation between $z(\boldsymbol{x}_i)$ of any two sample points can be expressed as a function of their spatial distance. The most widely used Gaussian correlation model is adapted as,

$$\boldsymbol{R}\left(z(\boldsymbol{x}_i), z\{(\boldsymbol{x}\}_j)\right) = exp\left(-\sum_{k=1}^{m} \theta_k \left|x_i^k - x_j^k\right|^{p^k}\right), \tag{5}$$

where x_i^k and x_j^k are the k^{th} components of the two sample points $\boldsymbol{x}_i$ and $\boldsymbol{x}_j$, m is the number of design variables. The p^k and θ_k are sample-adjusted interpolation parameters. The parameter p influences the smoothness of the correlation and θ_k controls the decay rate of correlation on different dimensions. From this, it is possible to construct n x n matrix of correlation functions between sample points as

$$\boldsymbol{R} = \begin{Bmatrix} R(\boldsymbol{x}_1\boldsymbol{x}_2), & \dots & R(\boldsymbol{x}_1\boldsymbol{x}_n) \\ \dots & \ddots & \dots \\ R(\boldsymbol{x}_n\boldsymbol{x}_2) & \dots & R(\boldsymbol{x}_n\boldsymbol{x}_n) \end{Bmatrix}. \tag{6}$$

Therefore, a set of variables $y(x_i)$, which are correlated throw matrix $\boldsymbol{R}$. These correlations depend on the distance between the sample points $\left|x_i^k - x_j^k\right|$and the parameter θ_k.

The likelihood function of the sample point can then be written as

$$L = \frac{1}{(2\pi\sigma^2)^{\frac{m}{2}}|\boldsymbol{R}|^{\frac{1}{2}}} exp\left[\frac{(\boldsymbol{Y}-\boldsymbol{F\beta})^T\boldsymbol{R}^{-1}(\boldsymbol{Y}-\boldsymbol{F\beta})}{2\sigma^2}\right], \tag{7}$$

where $\boldsymbol{F}$ is considered as a unitary vector $\mathbf{1}$ of a size equal to the number of samples. $|\boldsymbol{R}|$ is the determinant of $\boldsymbol{R}$ which is a function of θ_k. Thus, according to the maximum likelihood function method seeking the model parameters ($sigma$ and p) that maximize the probability model representing the function that originated the samples, this process called training

$$\widehat{\boldsymbol{\beta}} = \left(\frac{\boldsymbol{F}^T\boldsymbol{R}^{-1}\boldsymbol{Y}}{\boldsymbol{F}^T\boldsymbol{R}^{-1}\boldsymbol{F}}\right), \tag{8}$$

$$\hat{\sigma}^2 = \frac{((\boldsymbol{Y}-\boldsymbol{F\beta})^T\boldsymbol{R}^{-1}(\boldsymbol{Y}-\boldsymbol{F\beta}))}{n}. \tag{9}$$

The logarithm function concentrated likelihood can be written as

$$ln(L) \approx -\frac{m}{2}ln(\hat{\sigma}^2) - \frac{1}{2}ln|\boldsymbol{R}|. \tag{10}$$

Model training can be done by any optimization technique. Forrester *et al.* [21] recommended the use of a genetic algorithm due to its easy operation. Thus, to define function prediction (interpolation) using the statistical model the prediction point $\hat{y}$ is added to the

sample, increasing the correlation matrix using the previously adjusted parameters. The maximum likelihood is applied to the new sample, where only the value $\hat{y}$ is unknown, and the function is maximized. For any point x_0, following the principle that the predicted value for the point continues to maximize the augmented likelihood function of both the sample point and the new point, the predicted response value can be obtained by

$$\hat{y}(\boldsymbol{x}_0) = \boldsymbol{f}^T\widehat{\boldsymbol{\beta}} + \boldsymbol{r}^T(\boldsymbol{x}_0)\boldsymbol{R}^{-1}\left(\boldsymbol{Y} - \boldsymbol{F}\widehat{\boldsymbol{\beta}}\right). \tag{11}$$

where $\boldsymbol{r^T}(x_0)$ is a row vector of correlation function between the new point and each sample point as

$$\boldsymbol{r}^T(\boldsymbol{x}_0) = [\boldsymbol{R}(\boldsymbol{x}_0, \boldsymbol{x}_1), \cdots, \boldsymbol{R}(\boldsymbol{x}_0, \boldsymbol{x}_n)]. \tag{12}$$

Therefore, when the value of the i^{th} a sample point is predicted, since $\boldsymbol{r^T}(x_i)\boldsymbol{R}^{-1}$ equals the i^{th} order unit vector

$$\hat{y}(\boldsymbol{x}_i) = \boldsymbol{f}^T(\boldsymbol{x}_i)\widehat{\boldsymbol{\beta}} + y_i - \boldsymbol{f}^T(\boldsymbol{x}_i)\widehat{\boldsymbol{\beta}} = y_i, \tag{13}$$

which shows that the Kriging model predicts the real response value at the sample point, and it says the reason it can be considered an interpolation technique.

The Kriging model allows the calculation of an estimate for the error of the model answers. The estimate of the potential error in the predictor is inversely associated with the curvature of the concentrated likelihood logarithm function. A low curvature (flatter curve) suggests a high potential for error, whereas a high curvature (flat curve) suggests a low potential for error [46]. Due to the technique being based on a statistical model, the estimated error of a predicted value can be obtained, which shows the reliability of the approximation. The error can be used to evaluate where in the domain it is most advantageous to include a new sample to define the approximation. This technique is called the re-interpolation of the model. Thus, the mean squared error (MSE) of the predictor is denoted by

$$\hat{s}^2(\boldsymbol{x}) = \boldsymbol{\sigma}^2\left[1 - \boldsymbol{f}^T\boldsymbol{x}, \boldsymbol{r}^T\boldsymbol{x}\begin{bmatrix}0 & \boldsymbol{F}^T\\ \boldsymbol{F} & \boldsymbol{R}\end{bmatrix}^{-1}\begin{Bmatrix}\boldsymbol{f}(\boldsymbol{x})\\ \boldsymbol{r}(\boldsymbol{x})\end{Bmatrix}\right], \tag{14}$$

Assuming that the substitute model is a faithful representation of the original model, it then is possible to seek the minimizer through an inexpensive evaluation of the surrogate model until finding a global optimum. However, one should guarantee the best possible substitution of the original model, at least where the overall minimum is found. For this, it is important to identify the convex regions to reduce the metamodel error in these regions. One way to guarantee these minimum regions is by adding new infill points (IPs). In this way, it is shown greater reliability in the substitute model. These points are determined using only the metamodel information [21].

2.3. Efficient Global Optimization - EGO

A metamodel approximates a high-fidelity model of an experiment or physical phenomenon. The quality of a metamodel can be influenced by several factors, such as the degree of nonlinearity of the problem, the number of design variables, the technique of selection of sample points, and their uniformity throughout the design space [47]. This makes the construction of a metamodel a complex process. The challenge becomes even greater when it looks for the generation of a surrogate model with the lowest number of sampling points possible, further reducing the computational cost.

One way to get new Infill Points (IPs) and get global optimization is to focus on finding domain regions with some degree of uncertainty about the surrogate model. For this, the square root of the Mean Squared Error (RMSE) can be calculated as $\hat{s} = \sqrt{\hat{s}^2}(\boldsymbol{x})$. However, the metric to be chosen for IPs addition must contain a good balance between local and global search and involve the minimum value of the function already obtained [46]. To perform a search and infill strategy the goal is to position the next IP at the value of x that leads to an improvement on the best-observed value so far, y_{min}. Thus, by considering $\hat{y}(\boldsymbol{x})$ as the realization of a random variable, the expression of the probability of an improvement $\boldsymbol{I} = y_{min} - \hat{y}(\boldsymbol{x})$ upon y_{min}, results in a probability of improvement calculated using the error function as

$$P[I(\boldsymbol{x})] = \frac{1}{2}\left[1 + erf\left(\frac{y_{min} - \hat{y}(\boldsymbol{x})}{\hat{s}\sqrt{2}}\right)\right], if \;\; \hat{s}(\boldsymbol{x}) > 0 \tag{15}$$

However, instead of finding the probability that there is some improvement, it is possible to calculate the amount of improvement. One of the most common infill methods used is the Expected Improvement (EI). EI calculates how much improvement is expected to be

achieved by sampling at a given point. This technique was developed to be used in conjunction with the Kriging metamodel. The Expected Improvement is determined by

$$E[I(\boldsymbol{x})] = \begin{cases} (y_{min} - \hat{y}(\boldsymbol{x}))\Psi\left(\frac{y_{min} - \hat{y}(\boldsymbol{x})}{\hat{s}(\boldsymbol{x})}\right) + \hat{s}(\boldsymbol{x})\boldsymbol{\psi}\left(\frac{y_{min} - \hat{y}(\boldsymbol{x})}{\hat{s}(\boldsymbol{x})}\right), if\, \hat{s}(\boldsymbol{x}) > 0 \\ 0, if\, \hat{s}(\boldsymbol{x}) = 0 \end{cases} \quad (16)$$

where Ψ and ψ represent, respectively, the probability density function and the cumulative probability function of a normal distribution [48]. y and $\hat{s}$ are, respectively, the mean and the RMSE [21]. Then, the first term is the difference between the current minimum of the function y_{min} and the predicted value $\hat{y}(x)$. The second term represents the uncertainty of $\hat{y}(x)$reaching y_{min} [49]. The method associates different amounts of improvement or distances below y_{min}, with the RMSE variability over the metamodel domain.

In this criterion, each new point is positioned in the region where the expected improvement is maximum. The strategy of the criterion consists of considering the expected improvement null in the already known points, preventing the search in regions previously exploited, and certifying the convergence of the algorithm. Also, the magnitude of EI increases with $\hat{s}$, stimulating demand in lesser-known regions, and increasing with the $\hat{y}(\boldsymbol{x})$, favoring the search for regions where the predicted value is less than y_{min} [40].

Therefore, EGO selects input combinations based on the maximization of the EI. EGO uses the Kriging model to approximate the input/output function simulation. The Kriging predictor equals the simulation outputs for input combinations that have already been simulated. EGO estimates the EI through the Kriging predictor and the estimated variance of this predictor [23].

3. Materials and Methods

Figure 1 summarizes the combined numerical-experimental procedure. First, the design variables' limits are defined and the levels of variability on each of the design variables are quantified. The material properties and geometric dimensions of the composite material samples are collected as input data. The variability of the data is considered to determine the intact range of each design variable, *i.e.*, the variability of the manufacturing process. Design variables related to the geometry of the laminated composite plates are evaluated (Step 1), and the variables related to the material properties are taken from literature [17-18, 38, 50-54] (Step

2). In parallel, experimental modal analysis (Step 3) of the intact (undamaged) laminated composite plates is used as a guideline for the numerical simulation. An impact test (Step 4) using a drop toweris carried out to impose damage on the plates. Damage affects the structural characteristics of the plates, including their resonance frequencies. Modal analysis experiments of intact (undamaged) and damaged structures contain information on the damage type and the influence of this damage on each mode.

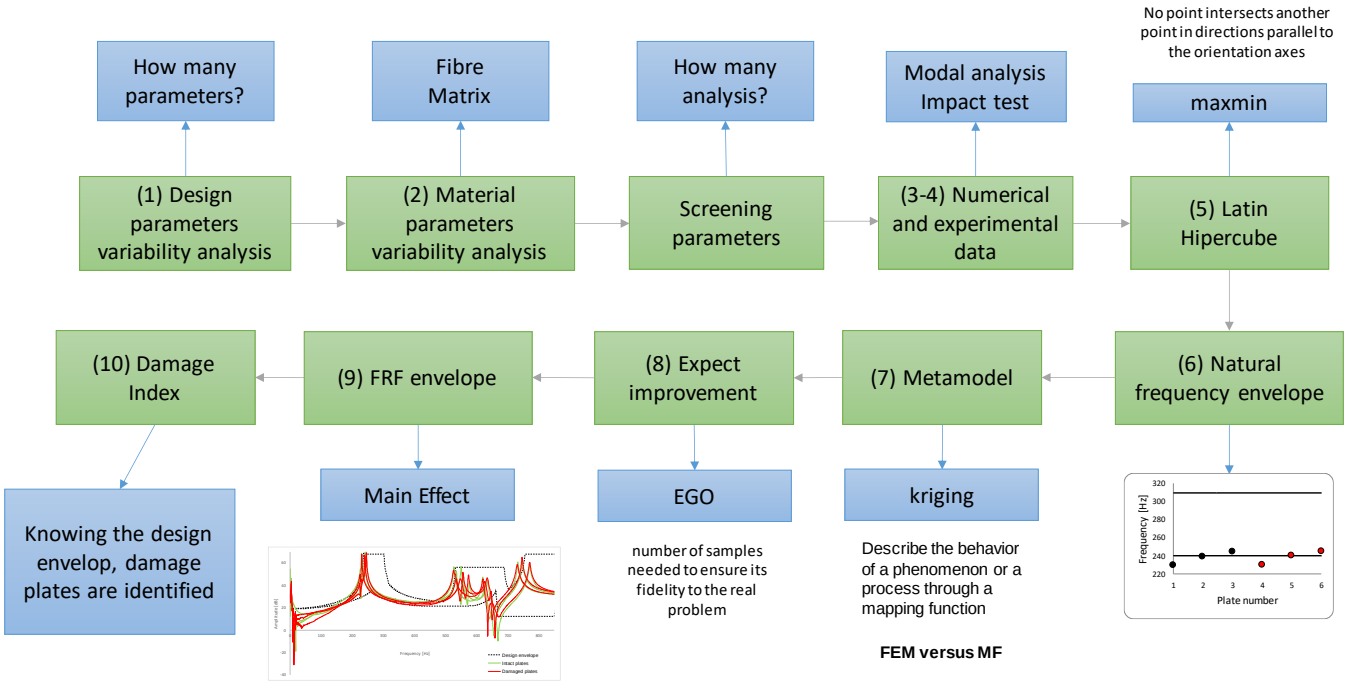

Figure 1. Numeric-experimental procedure

A Latin Hypercube scheme (Step 5) is used to conduct the logic of the test sequence. The LH determines the value of each design variable within the range considered intact obtained by the previous step. With the design of experiments (DoE) built, the next stage consists of running simulations. The finite element analysis (Step 6) is performed to determine the natural frequencies for each test line of the input variables whose values were determined by the Latin Hypercube in the previous step. The commercial *Abaqus*® finite element software is used for setting and solving models. Automated data handling is done using a Python routine.

In Step 7, with the input and output data, the Kriging metamodel is built. This numerical model replaces the finite element model in Step 6. In other words, this model provides a simplified way to obtain natural frequencies without explicit execution of any *Abaqus*® models. In addition to the sample points provided, the model predicts intermediate points. Six metamodels are built for each group of the plate/material that consists of one metamodel for

each natural frequency. The Kriging metamodel is built from a computational routine written in Python. However, this model can be contaminated with errors that can be caused by the lack of sampling points in specific regions. To overcome this issue (Step 8), the Efficient Global Optimization (EGO) algorithm through Expected Improvement (EI) is used to predict regions that need the inclusion of Infill Points (IP) to rebuild the Kriging metamodel. The highest EI average between Kriging models is considered for choosing the point to be inserted. The EGO is done using a computational routine in Python as well. To ensure the correctness and reliability of the code routine, a crucial step in the validation process involved cross-referencing the outcomes with the results obtained by Forrester *et al.* [21].

The numerical results are used to create the manufacturing envelope (Step 9), which characterizes the set of composite plates evaluated in the DoE process. The envelopes generated by numerical and experimental FRFs are compared, and the results are discussed in terms of the potential and limitations of the proposed procedure. Finally, based on intact and damaged experimental results, the values of the Damage Index (Step 10) are quantified.

4. Design variables analysis and material properties

Mechanical tests are performed on a set of 10 composite plates made of Glass Fibre Reinforced Polymer (GFRP) manufactured by a modified VARTM (Vacuum Assisted Resin Transfer Molding) process. The GFRP specimens were manufactured and tested in the Aeronautical Structure Laboratory at the Sao Carlos School of Engineering of the University of São Paulo. The composite plates are made of sixteen layers with $[(45/-45/0/90)_2]_s$. The first three samples (P01 through P03) are made from a unidirectional fabric (UD) of 140 g/m², and the remaining five (P06 through P08) from a bidirectional fabric (BD) of 83 g/m². Both fabrics are supplied by the manufacturer Texiglass/Brazil, and they are named [WRU-140] and [WR-83]. The polymer matrix was an epoxy resin [1564 BR (85 % w/w)], which uses a hardener [REN HY 150 BR (15 % w/w)] during the cure cycle. This take 8 hours in vacuum bag molding and ambient temperature. Figure 2(a) shows a unidirectional GFRP composite sample, and Figure 2(b) shows a bidirectional one.

The plates have a nominal length of 150 mm and a width of 100 mm. The thickness is 1.7 mm for unidirectional (UD) samples, and 1.6 mm for bidirectional (BD) samples. To conduct the DoE process, the upper and lower limits values of the design variables must be defined. The quality of the DoE representation is improved using reference data to define these boundaries [38]. The upper and lower limit values of the geometric [50] and material [51-54]

parameters are based on the standard deviation (SD) described in the literature [38]. It was assumed 3-sigma interval, which is related to the standard deviation. However, the upper and lower values for thickness were obtained evaluating the distribution provided by the 3D scanner. Where a normal distribution has been observed. Therefore, the upper and lower values for the thickness range was defined in a way that, 99.7% of the measured values were into these boundaries. Sutcliffe *et al.* [54] evaluate the fibre orientation considering the resin transfer moulding process (RTM), and obtain a standard deviation of 0.6 degree for in-plane orientation. As shown in the literature [38], three standard deviations (3σ) are considered to determine the maximum and minimum values of each angle. Tables 1 and 2 show the design variable analysis, considering the mean, upper, and lower values for the GFRP-UD (Table 1), and GFRP-BD (Table 2) composite plates, respectively.

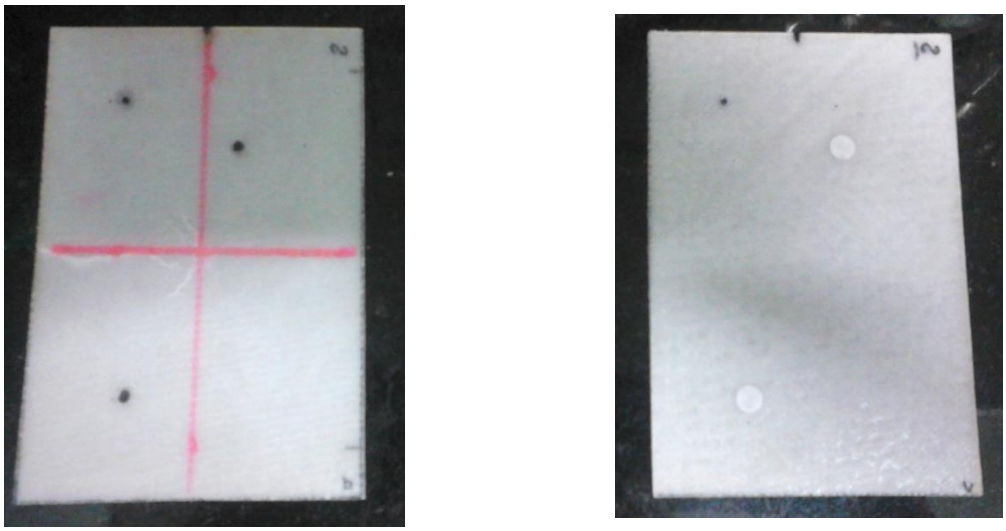

(a) (b)

Figure 2. GFRP composite samples [50]: (a) UD fabric; (b) BD fabric.

Table 1. Design variables and its levels from GFRP-UD with $[(45/-45/0/90)_2]_S$

Variable	Reference	Mean value	Lower	Upper	Unit
Length (L)	[50]	152.60	148.54	156.68	mm
Width (W)	[50]	101.20	96.31	106.90	mm
Thickness (t)	[50]	1.70	1.60	1.80	mm
θ_0 (0°)	[54]	0	-1.8	1.8	degrees
θ_{90} (90°)	[54]	90	88.2	91.8	degrees
θ_{45} (45°)	[54]	45	43.2	46.8	degrees
θ_{-45} (−45°)	[54]	-45	-46.8	-43.2	degrees
Young's Modulus longitudinal (E_{11})	[51]	38.60	37.84	39.36	GPa
Young's Modulus transversal ($E_{22} = E_{33}$)	[51]	13.61	12.67	14.55	GPa
Shear Modulus in plane 1-2 ($G_{12} = G_{13}$)	[51]	7.14	6.90	7.38	GPa
Shear Modulus in plane 2-3 (G_{23})	[52]	2.30	2.06	2.54	GPa
Poisson's ratio in plane 1-2 ($\nu_{12} = \nu_{13}$)	[51]	0.353	0.327	0.378	-
Density (ρ)	[51]	1616.40	1500.16	1732.64	Kg/m^3

Table 2. Design variables and its levels from GFRP-BD with $[(45/-45/0/90)_2]_S$

Variable	Reference	Mean value	Lower	Upper	Unit
Length (L)	[50]	149.40	147.93	150.87	mm
Width (W)	[50]	100.56	96.48	104.64	mm
Thickness (t)	[50]	1.60	1.50	1.70	mm
θ_0 (0°)	[54]	0	-1.8	1.8	degrees
θ_{90} (90°)	[54]	90	88.2	91.8	degrees
θ_{45} (45°)	[54]	45	43.2	46.8	degrees
θ_{-45} (−45°)	[54]	-45	-46.8	-43.2	degrees
Young's Modulus longitudinal (E_{11} = E_{22})	[53]	19.1	17.19	21.01	GPa
Young's Modulus transversal (E_{33})	[53]	1.8	1.62	1.98	GPa
Shear Modulus in plane 1-2 (G_{12})	[53]	2.9	2.61	3.19	GPa
Shear Modulus in plane 2-3 (G_{23} = G_{13})	[53]	1.6	1.44	1.76	GPa
Poisson's ratio in plane 1-2 (ν_{12})	[53]	0.11	0.10	0.12	-
Density (ρ)	[50]	1722.0	1668.9	1775.1	Kg/m^3

5. Experimental Modal Analysis

The experimental analysis is carried out via vibration tests on composite plates hung by elastomeric wires to simulate "free-free" boundary conditions. The natural frequencies and the Frequency Response Functions (FRFs) for undamaged (intact) and damaged (impact) plates are obtained using two accelerometers. The accelerometers are model 352A24 and model 352C22 for lightweight structures. Accelerometer 1 (sensitivity 99.6 mV/g) is mounted at position 2, and accelerometer 2 (sensitivity 9.57 mV/g) is mounted at position 3 (Figure 3). Force excitation by impact hammer is applied in position 1. The positions of the accelerometers are selected based on the previous modal analysis, avoiding nodal lines and considering the first six mode shapes [18], [50].

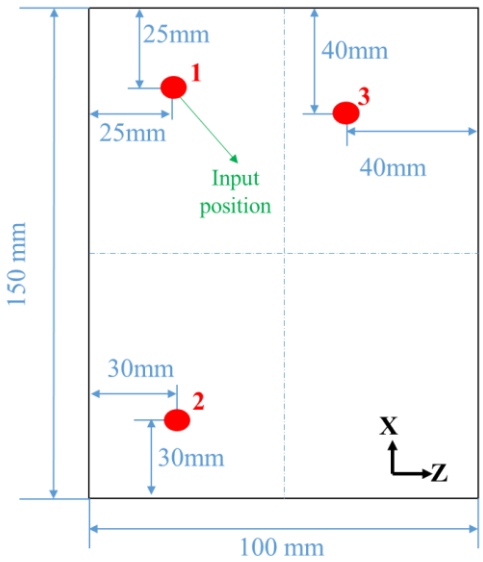

Figure 3. Positions of the accelerometers (points 2 and 3) and impact impulse (point 1) [50]

Figure 4 shows all data acquisition setups used in the experiment for damage identification. The specimen is suspended by elastomeric wires to simulate “free-free” boundary conditions. The accelerometers and the hammer are linked to an LMS SCADAS Mobile equipment, which is controlled by the Test.Lab software (LMS Test.Lab). The LMS SCADAS Mobile is plug-and-play equipment and it has a multifunction analogy, digital, and timing I/O board for USB bus computers. Each signal consists of 2048 points and sampling is done from 0 Hz to 1024 Hz. The frequency band of 850 Hz is selected to calculate the damage index (damage metric) by vibration-based method for the first six natural frequencies of the structure. The number of averaging individual time records is selected to be five to reduce the variation effects. This analysis can be evaluated by comparing not only the FRFs but also the coherence values. The dataset contains mode shape and FRFs, which include information on natural frequencies and damping factors.

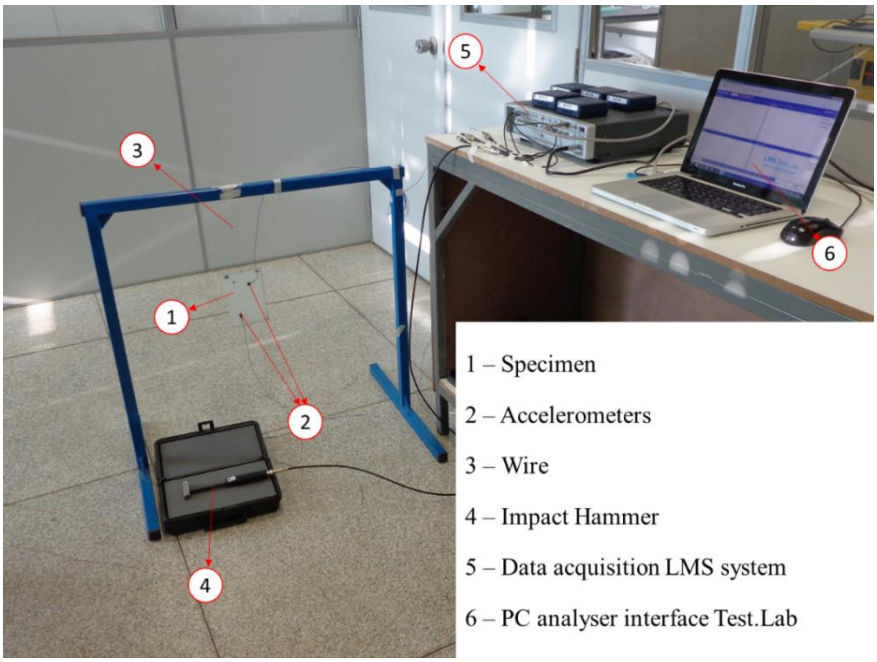

Figure 4. Experimental setup for modal analysis [50]

6. Damage plates by impact loading

An impact load inflicts damage to the composite structures [55-59]. A drop tower is used to damage the composite plates. The drop tower apparatus consists of two vertical bars, which guide the falling weight during the test, producing a normal impact loading with a hemisphere impactor. According to ASTM 7136M [60], the damage resistance properties generated by this test method are highly dependent upon several factors, which include specimen geometry, lay-

up, impactor geometry, impactor mass, impact force, impact energy, and boundary conditions. Figure 5 shows the drop tower apparatus and the test specimen mounted in the device ASTM 7136M on the basis of the drop tower. This test method determines the damage resistance of multidirectional polymer matrix composite laminated plates subjected to a drop-weight impact event. The tests are carried out using an aluminium round impactor head with a diameter of 16 mm, impactor weight of 0.074 kg, and are performed at the Aeronautic Structure Laboratory (University of Sao Paulo). In these experiments, the average potential energy level of the drop-weight used in the impact tests is set to 8.9 J (drop height of 1 m) for all plate sets [50].

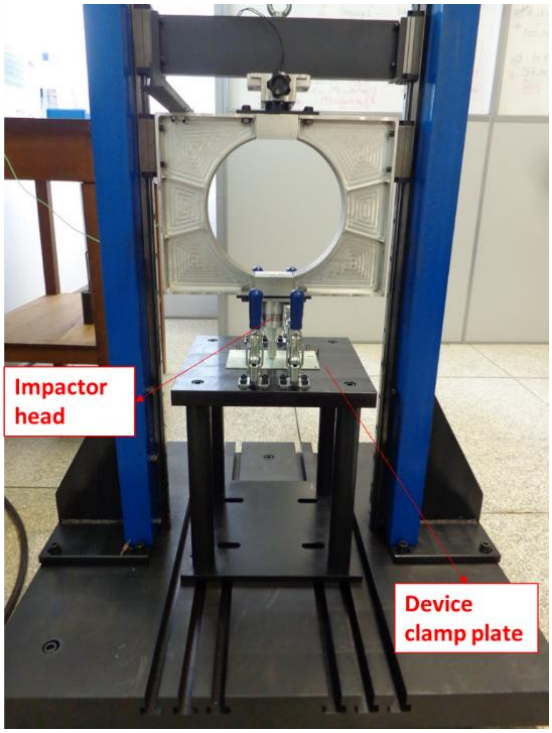

Figure 5. Drop test setup: Normal impact (by using a hemisphere impactor) on the GFRPcomposite plate [50]

7. Dynamic Numerical Analysis

Finite element models of composite plates are developed using the *Abaqus*® software, which incorporates subroutines written in Python. The set of input-output data are the initial samples in the Kriging metamodel. Specifically, the finite element model is used in different stages of the procedure. First, the computational model is used to generate the initial sample data as a basis for the Kriging metamodel. Second, the computational model is used each time when the EGO model requests a new infill point to compose the Kriging Metamodel. In addition, the computational Frequency Response Function (FRF) is obtained to define the envelope considered without manufacturing defects.

The finite element models of the composite plates feature a mesh of quadrilateral 8-node shell elements defined as S8R5. This element presents an 8-node isoparametric doubly curved thin shell, reduced integration, and five degrees of freedom (DOF) per node (three translations and two rotations) [61]. The plate is modelled with 4.287 quadrilateral elements and 12.951 nodes. Numerical simulations are run to obtain the natural frequencies and FRFs under "quasi" free-free boundary conditions, because the elastic wires attached to the composite plates are simulated as used in the vibration experimental tests.

The accelerometers have a very small mass when compared to the mass of the structure. No added mass is included in the numerical modal analysis. As commented earlier, one tip of the elastic wire with very low stiffness (10 N/m) is attached to the composite plate. The other tip of the elastic wire is modelled with fixed translations (Ux, Uy, Uz) and rotations (Urx, Ury, Urz). To generate the envelope, dynamic implicit analyses are done to obtain the FRFs (Figure 6). The same boundary conditions described previously for modal analyses are applied to the dynamic analyses. An impulse loading is applied on the surface of the plate simulating the excitation of a hammer at the same loading point of experimental plates. The input signal is a transverse force of amplitude equal to 1 N. The frequency range of the force is 0 to 1024 Hz. Damping coefficients are identified experimentally from the modal analyses of the plates.

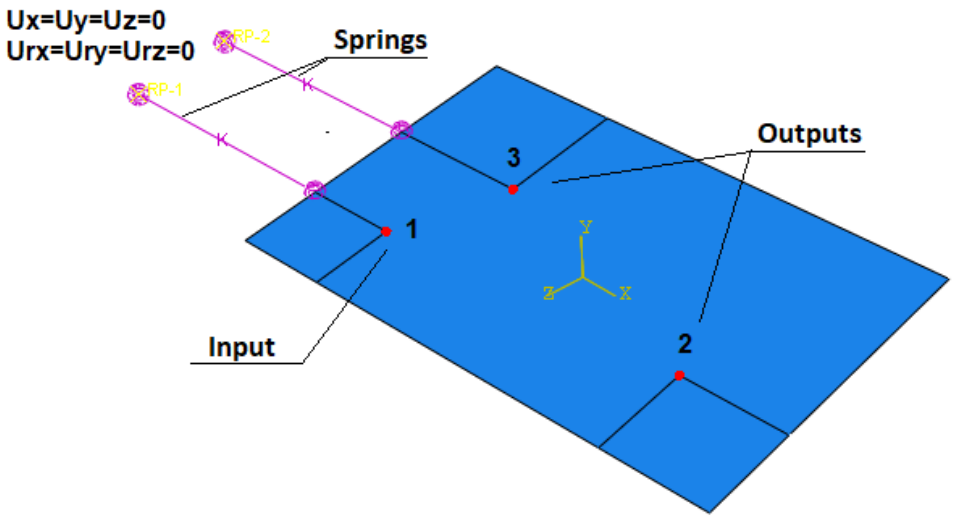

Figure 6. Boundary conditions considered in the numerical analysis

Table 3 shows the mean value and the standard deviation of the damping coefficients for each mode. In general, the composite properties result in greater damping with higher resin content during the manufacturing process. The mean value of damping coefficients of

experimental plates is in the finite element models. Frequency Response Functions (FRFs) are obtained from the same point to the experimental sensor using the numerical model (**Erro! Fonte de referência não encontrada.**). Figure 7 shows the first six modes, which are the 1st bending mode, 1st torsion mode, 2nd torsion mode, 2nd bending mode, 3rd torsion mode, and 4th torsion mode, which are the same for both, UD and BD, plate configurations.

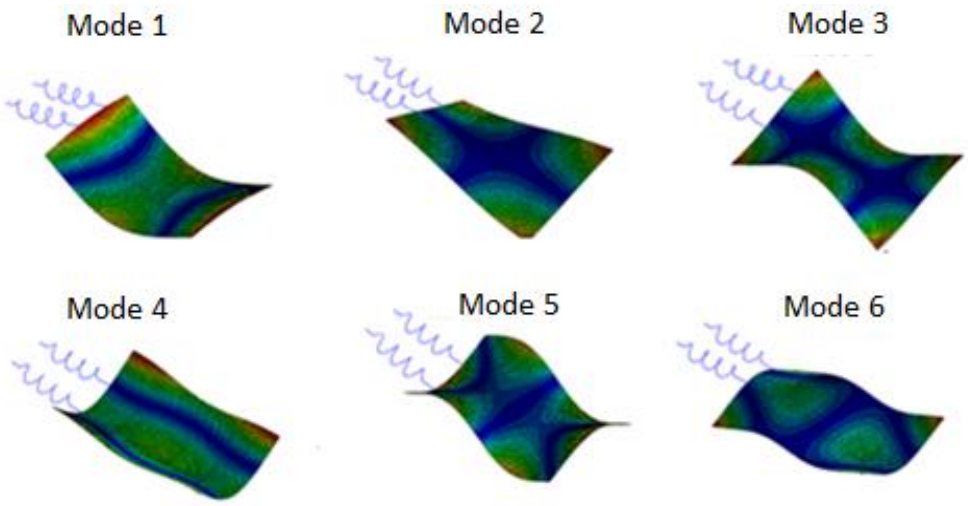

Figure 7. Vibration modes of GFRP-UD and GFRP-BD plates

Table 3. Damping coefficient obtained from the modal analysis of GFRP plates

	ξ_1	ξ_2	ξ_3	ξ_4	ξ_5	ξ_6
P01 – UD	0.36	0.21	0.26	0.23	0.25	0.24
P02 – UD	0.48	0.21	0.24	0.22	0.31	0.23
P03 – UD	0.32	0.21	0.20	0.24	0.30	0.27
Mean Value	**0.39**	**0.21**	**0.23**	**0.23**	**0.29**	**0.25**
Standard deviation	**0.08**	**0.00**	**0.03**	**0.01**	**0.03**	**0.02**
P06 – BD	0.28	0.24	0.27	0.33	0.23	0.28
P07 – BD	0.44	0.27	0.28	0.32	0.23	0.44
P08 – BD	0.36	0.25	0.25	0.39	0.25	0.36
Mean Value	**0.36**	**0.25**	**0.27**	**0.33**	**0.23**	**0.36**
Standard deviation	**0.08**	**0.02**	**0.02**	**0.04**	**0.01**	**0.08**

8. Metamodel Kriging and EGO

According to Xiao *et al.* [62], for all plates (samples) using one of the existing designs of experimental methods, if the dimension of input variables is less than 10, the initial training sample (n_s) is equal to 12; otherwise, n_s is equal to the number of variables plus 5 (five). Considering the input parameters for both plate configurations, 18 initial samples are defined, and the training of the Kriging metamodel is started. Figure 8 presents a detailed flowchart of the steps performed during metamodel training to find an optimized numerical model. It is

observed that the calculation of output variables (first six natural frequencies) is performed by the Finite Element Method.

After reading the inputs and outputs, the first step is to provide the number of analysed frequencies to the program code. For the plates, this number is defined as equal to 6. It is also defined that the number of analysis points "*p*" during the Kriging process, and its optimization would be 100 samples, which corresponds to the addition of 100 points suggested to the model. These samples are obtained through the Latin Hypercube algorithm. This value is a balance between precision, robustness, and resource efficiency, ensuring that the design is both effective and practical for real applications.

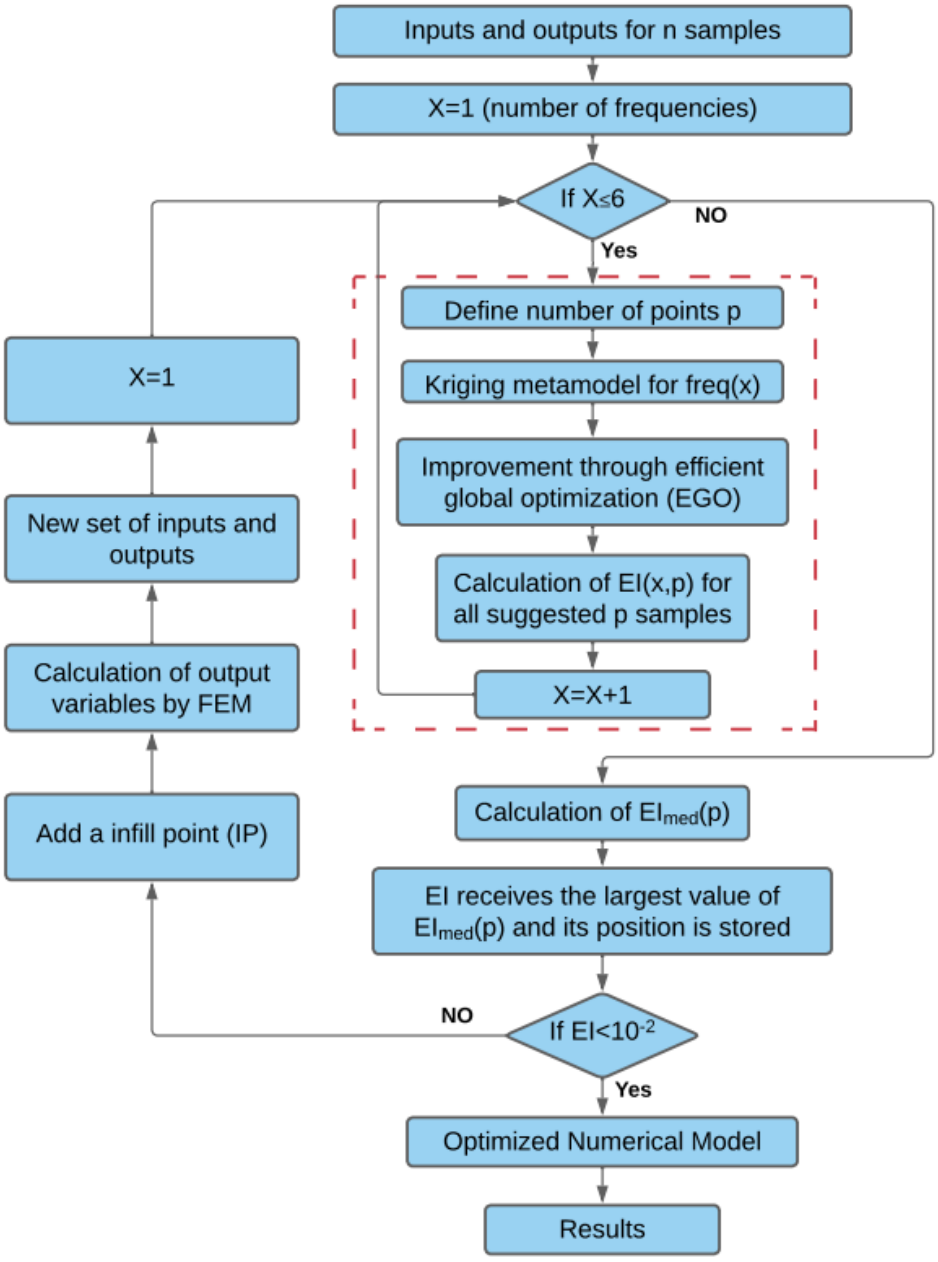

Figure 8. Kriging metamodel flowchart: Training to find an optimized numerical model

Based on this information, the Kriging metamodel is trained for the set of inputs to obtain the first output frequency. Once the training of the Kriging model [63] is complete, a numerical model is generated and subsequently improved through Efficient Global Optimization (EGO) [21, 64]. The Expected Improvement (EI) [21, 65] metric is used. The EI metric is calculated for the first output frequency for all 100 suggested samples. At the end of the process, a vector with 1×100-dimension containing the EI values for the first frequency is stored.

The Kriging process with global optimization is repeated for the other output frequencies (steps involved by the dashed lines in the flowchart). At the end of the process, 6 metamodels are created, resulting in a 6×100 matrix. The average of the EI values for each of the 100 points is calculated and stored in the EI_{med} vector of dimension 1×100:

$$\boldsymbol{EI_{med}}(p) = \frac{\sum_{x=1}^{6} EI(x,p)}{6} \tag{17}$$

After the EI_{med} vector is calculated, the highest EI_{med} value is stored in the EI_{max} variable. If the value obtained for the EI_{max} metric is greater than an established limit, which was set to be 10^{-2}, a new Infill Point is added. With the addition of this point, the input variables are stored, and used in the numerical model to obtain the output variables via the Finite Element Analysis (FEA). This set of inputs and outputs is added to the 18 samples, and a new iteration is started. When the value obtained for the EI metric is lower than 10^{-2}, the variables of the optimized numerical model are obtained, and the dynamic analysis could be carried out to provide the Frequency Response Functions for determining the upper and lower frequency limits via FEA, again.

9. Manufacturing Defect

After the Kriging step the model is optimized. The output data (frequencies) are analyzed to retain the maximum and minimum values. These values are obtained based on the values provided by the support points, assuming that there are no maximum and minimum frequency points between these points. The maximum and minimum values for each frequency can be contained in different samples. As a result, these values are normalized and the maximum and minimum mean value is adopted as a criterion for selecting the limit samples. With the limits defined, the input data for the maximum and minimum frequencies and the mean value of the

experimental damping are used to obtain the numerical responses (FRFs). The computational FRFs are plotted, and the valleys and peaks are linked to provide the design envelope. The FRFs for undamaged plates are added to the graph in order to detect manufacturing defects. If a sample has its FRF within the established limits, that sample would be considered intact ("without defects"). The flowchart in Figure 9 illustrates the successive steps.

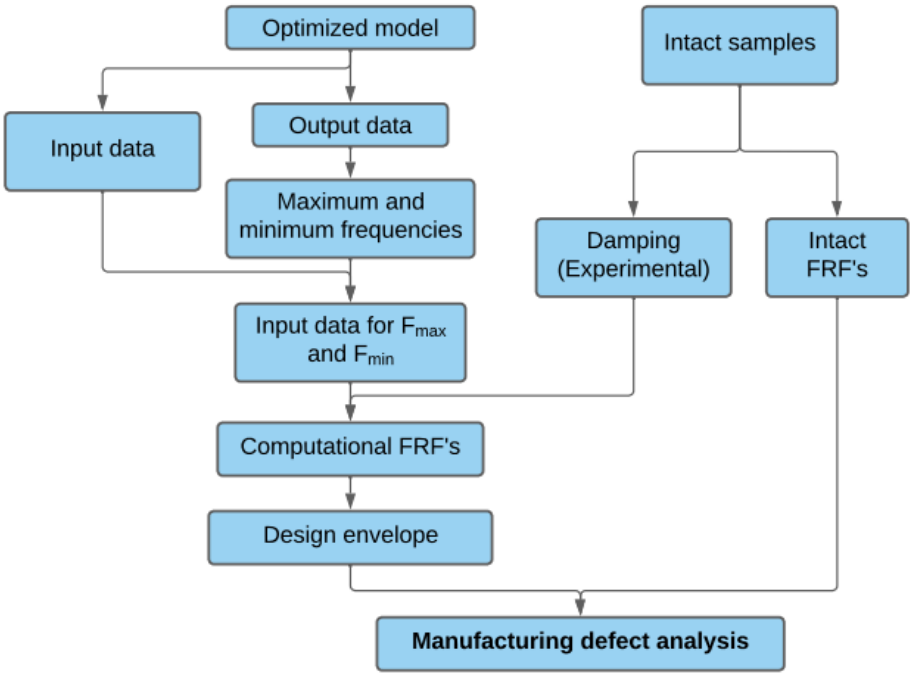

Figure 9. Manufacturing defect analysis flowchart

10. Damage Analysis

The detection of damage in composite structures requires the comparison of data from intact ("without defects") and damaged samples. Damages in the samples is caused by impact loading. More information about the damage can be found in the literature [17-18], [50].

Initially, the natural frequencies and FRFs of the intact and damaged samples are directly compared. However, those comparisons do not allow for effective detection of damage, as there are cases where the natural frequencies of the damaged samples are within the range of the intact ones, and the FRFs of both samples are similar. A Damage Index (DI) is an objective indicator of one response set with respect to another one. It is based on the amplitude and phase of the FRFs from intact and damaged samples, defined as:

$$DI_{GAP_j} = \left| 1 - \frac{\sum_{\omega} \left(H_{jk}^{d}(\omega) \cdot P_{jk}^{d}(\omega) \right)}{\sum_{\omega} \left(H_{jk}^{i}(\omega) \cdot P_{jk}^{i}(\omega) \right)} \right| \quad (2)$$

where the superscripts *i* and *d* represent the undamaged (intact) and damaged structures, respectively. And, the subscripts *j* and *k* denote the location of measure and force, respectively. *H(ω)* denotes the amplitude, *P(ω)* is the phase, and *ω* is the frequency range. More details about the DI, such as the formulation, can be found in the literature [17-18], [50]. In a general way, the expression of the DI returns a value equal to zero when the structure does not change its structural behaviour, *i.e.* when there is no damage The value of the DI increases as the structural behaviour changes.

11. Results and Discussion

From Latin Hypercube (LH), the values of the design variables are obtained in each of the 18 test rounds. The values are based on design variable limits and LH matrices. The LH matrix is converted into a matrix with corresponding values for each design variable in each of the 18 rounds as input to the *Abaqus*® software. Each input generated by the LH results in the respective natural frequency output. The inputs and outputs set are used as a sample basis for the Kriging metamodel.

Infill points (IP) are included for GFRP plates. This inclusion occurs through point-to-point selection by the EI suggestion. With each new IP, Kriging metamodels are retrained until reaching the EI stop criterion $EI < 10^{-2}$. There are six natural frequencies of interest, corresponding to the first six modes of vibration (Figure 7). Once the computational model is trained with the infill points (IP) suggested by the EI, the ability to be used as a tool for assessing the quality of the composite plates is evaluated. Among the infill points (IP) used for training the metamodel, those that generate the minimum and maximum numerical natural frequencies as a training response are used as the basis for analysis. Each of these two IPs is composed of an input set and an output set. Specifically, 18 inputs to UD and BD composite plates are used, which are the design variables, and 6 outputs, which are the first six natural frequencies of composite plates.

11.1. GFRP-UD Composite Plates

The set of infill points added to the GFRP-UD plates for Kriging training by the EI method is shown in Figure 10. The maximum EI value per training determines the IP choice. The value of the first EI started at 1.7431, after that, another 31 points are added. The 31st EI value is 0.0127. In total, 49 points are used as a basis to construct the approximate function of the Kriging metamodel. Figure 11 shows a graphical representation of the numerical values of 49 frequency points. The vertical axis of the boxplot represents the natural frequency values for all points added by the EI, and the horizontal axis represents the first six natural frequencies. The observations that are above or below the central vertical lines are called outliers, that is, they are observations that are too high or too low for the pattern observed in the data, and are represented by points. The "X" represents the mean value and the central horizontal bar represents the median value of the quantitative variable. It is observed that the distribution is negatively skewed *i.e.*, the median lies closer to the third quartile. This demonstrates that the mean is less than the median, the frequencies tend towards the lower limit of the design parameters.

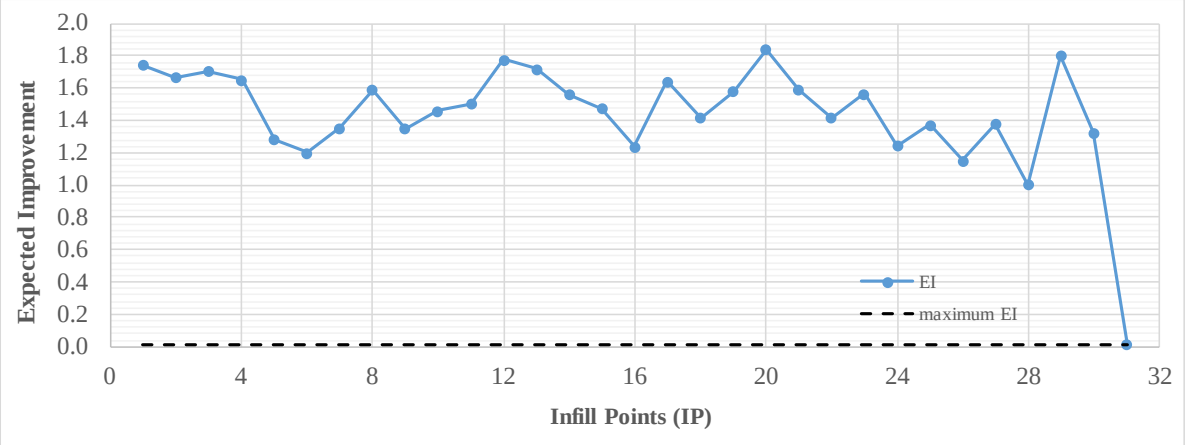

Figure 10. Expected Improvement (EI) evolution for GFRP-UD properties

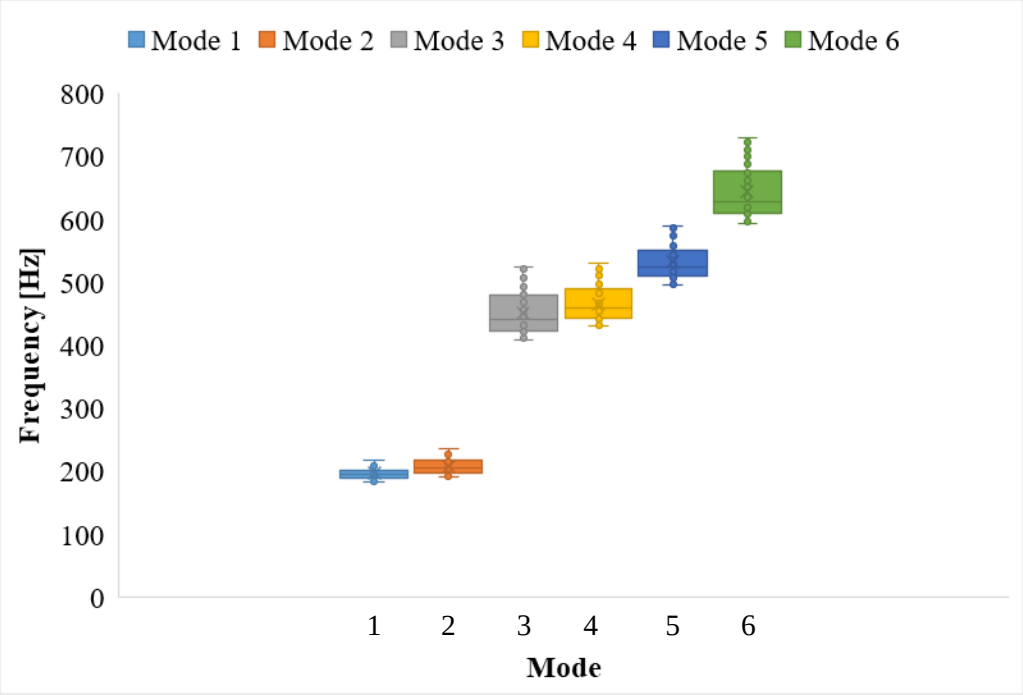

Figure 11. Expected Improvement (EI) evolution for GFRP-UD properties

At the end of the numerical model optimization, the values of the first six frequencies are analysed for each point. It is verified through normalization that for the minimum frequency, the chosen point presents almost all the minimum values between the points of the model, except for the frequencies at points 1 and 4. For the maximum point, only frequencies at points 1 and 5 do not present the maximum value, but the normalized values for the frequencies at 1 and 4 (minimum) are very close to zero and frequencies at 1 and 5 (maximum) to one. Table 4 presents the two points selected for the limits, as well as the values of the normalized frequencies.

Table 4. Maximum and minimum limits for the natural frequencies of the GFRP-UD plates

Frequency	$f(1)$	$f(2)$	$f(3)$	$f(4)$	$f(5)$	$f(6)$
Minimum	237.4	245.4	546.4	560.8	654.6	769.4
Maximum	295.7	311.3	696.2	772.5	815.2	1013.8
Normalized minimum	0.009	0.000	0.000	0.016	0.000	0.000
Normalized maximum	0.987	1.000	1.000	1.000	0.984	1.000

With the frequency limits defined by the computational mode, graphs are created containing the intervals of natural frequencies for undamaged samples. Figure 12 presents the maximum and minimum limits obtained by the computational model for the first six natural frequencies and six experimental samples (3 for intact and 3 for damaged structure).

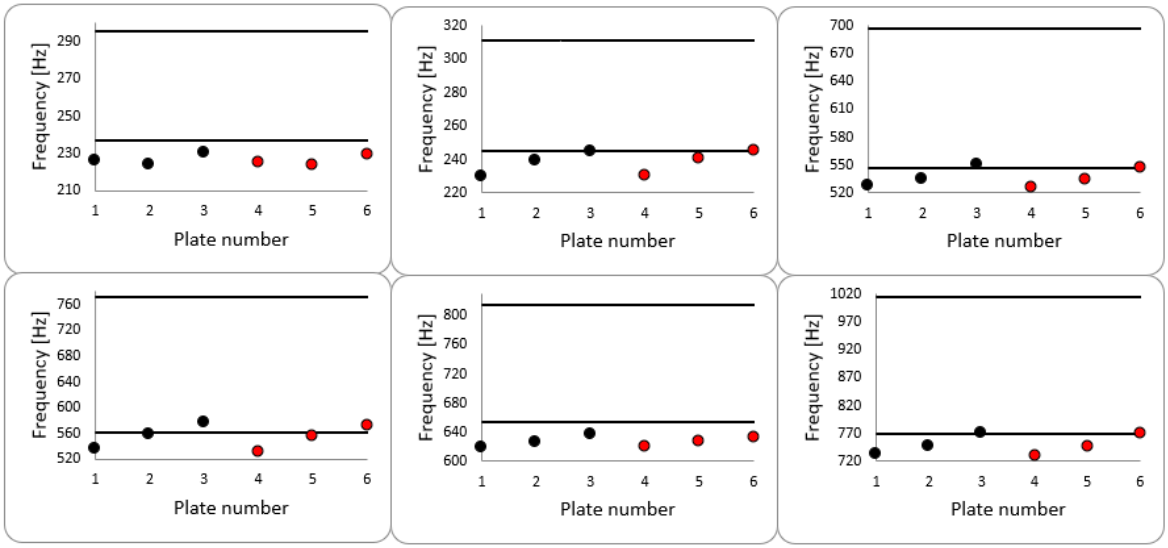

Figure 12. Natural frequency limits and experimental results, intact (black) and damaged (red), for the GFRP-UD plates

The first 3 samples are considered intact and the last 3 have some kind of impact damage. It is observed that almost all intact and damaged samples were below the limits established for each frequency. Thus, intact samples have some manufacturing defects. It is observed that intact and damaged samples 1 and 4, 2 and 5, and 3 and 6 had similar values for their natural frequencies.

After analysing the frequency range, the FRFs are obtained FE analysis. Figure 13 shows the envelope for intact samples created from these points, together with the FRFs of the 6 plates analysed. For this envelope, the data extracted from accelerometer at point 2 and the hammer impact at point 1 are considered. The intact plates are at the lower limit of the design envelope, confirming that they have problems in the manufacturing process. Small differences between intact and damaged FRFs are noticed around 550 and 600 Hz. Based on the FRFs presented by intact and damaged plates, it becomes difficult to define which samples are damaged by impact.

An envelope is also created for the data obtained from the accelerometer at point 3 and the hammer impact at point 1 shown on the plate. Figure 14 presents the design envelope together with the FRFs of the 6 analysed plates. For this case, the intact plates seem to at the lower limit of the proposed envelope interval, showing the presence of manufacturing defects. When verified between the FRFs of intact and damaged plates, FRFs peaks of the damaged structure are different from the intact ones in the ranges from 450 to 750Hz.

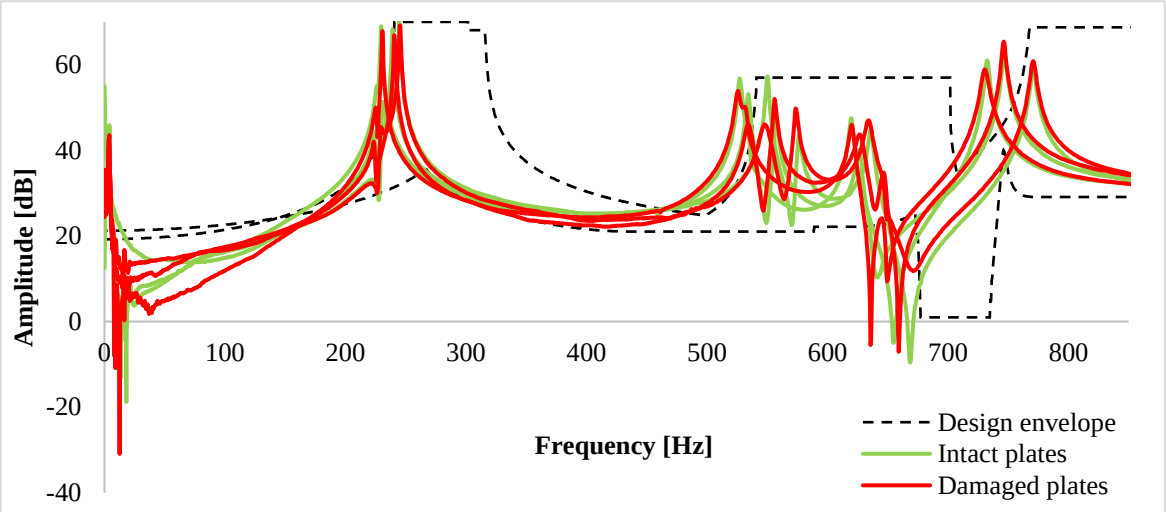

Figure 13. FRFs (H_{21}) envelopes for GFRP-UD plates

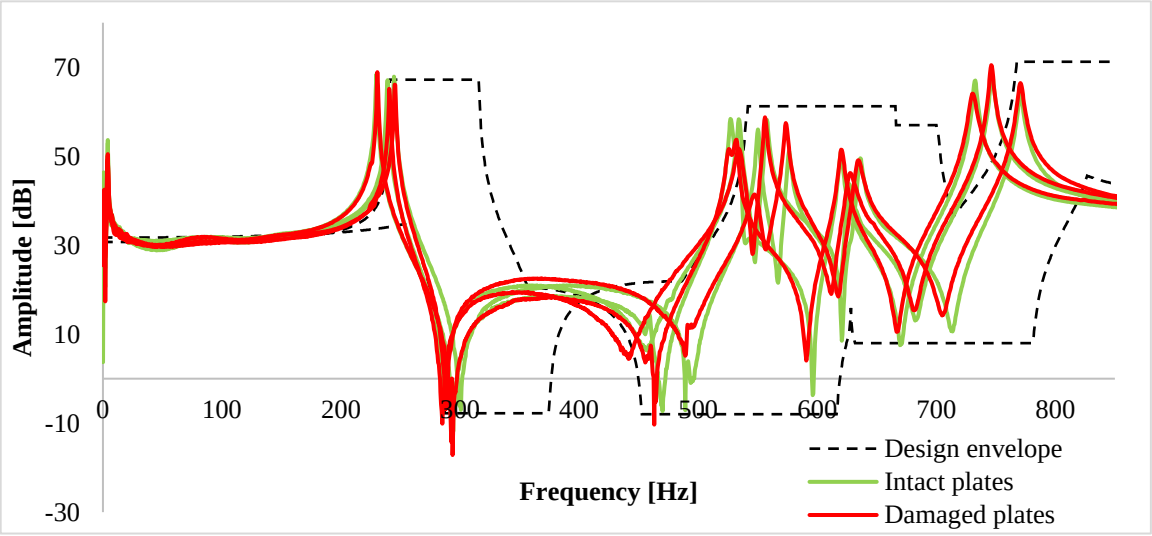

Figure 14. FRFs (H_{31}) envelopes for GFRP-UD plates

Finally, an analysis of the damage indices is carried out as presented in Eq. (2). Table 5 presents the damage indices found for the 3 plates analysed. It can be seen that the damage indices present higher values for the data analysed through the accelerometer 3, similar to what was observed in the previous FRFs, demonstrating the presence of the damage.

Table 5. Damage indices obtained for GFRP-UD plates

Frequency interval analyzed: 0 a 1024 Hz				
Plate	**H_{21}**	**H_{31}**	**Mean**	**Standard deviation**
1	2.632	2.146	2.389	0.243
2	0.149	1.003	0.576	0.427
3	1.205	1.871	1.538	0.333

11.2. GFRP-BD Composite Plates

A set of points are added to Kriging training of the GFRP-BD plates by the EI method as shown in Figure 15. The maximum EI value per training determines the IP choice. The value of the first maximum EI started at 0.4742, after that, another 31 points were added, besides 18 points of initial support. Due to changes in the approximate function of the Kriging metamodel, on the 14th ($EI_{IP=14} = 3.3868$) points EI peak occurred. The 31st EI value is 0.01822. In total, 49 points were used as a basis to construct the approximate function of the Kriging metamodel. Figure 16 shows a graphical representation of the numerical values of 49 frequency points. as in the UD case, it is possible to observe that the frequencies tend towards the lower limit of the design parameters.

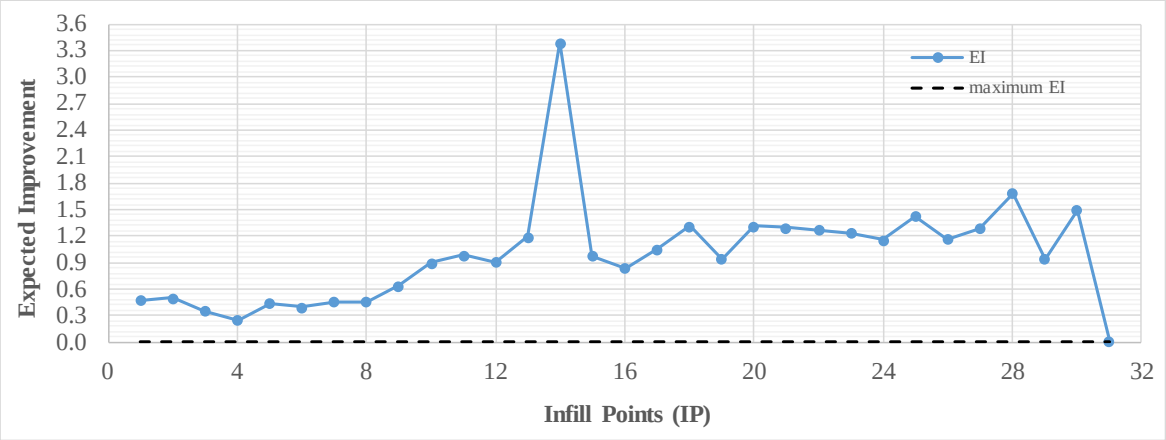

Figure 15. Expected Improvement (EI) evolution for GFRP-BD properties

At the end of the numerical model optimization, the values of the first six frequencies, the same UD plates, were analysed. As in the previous case, the maximum and minimum values for each of the frequencies were verified at different points. Thus, when performing the normalization of frequencies, a null value was verified for almost all values of minimum frequencies (except for the frequency at 2, 3 and 6) and a unit value for almost all values of maximum frequencies (except for the frequency at 1). Table 6 presents the two selected points, as well as the values of the normalized frequencies.

Based on the frequency limits defined by the computational mode, graphs were generated containing the frequency intervals of intact samples. Figure 17 presents the maximum and minimum limits obtained by the computational model for the first six frequencies and six experimental samples. The first 3 samples are considered intact and the last 3 have some kind of impact damage.

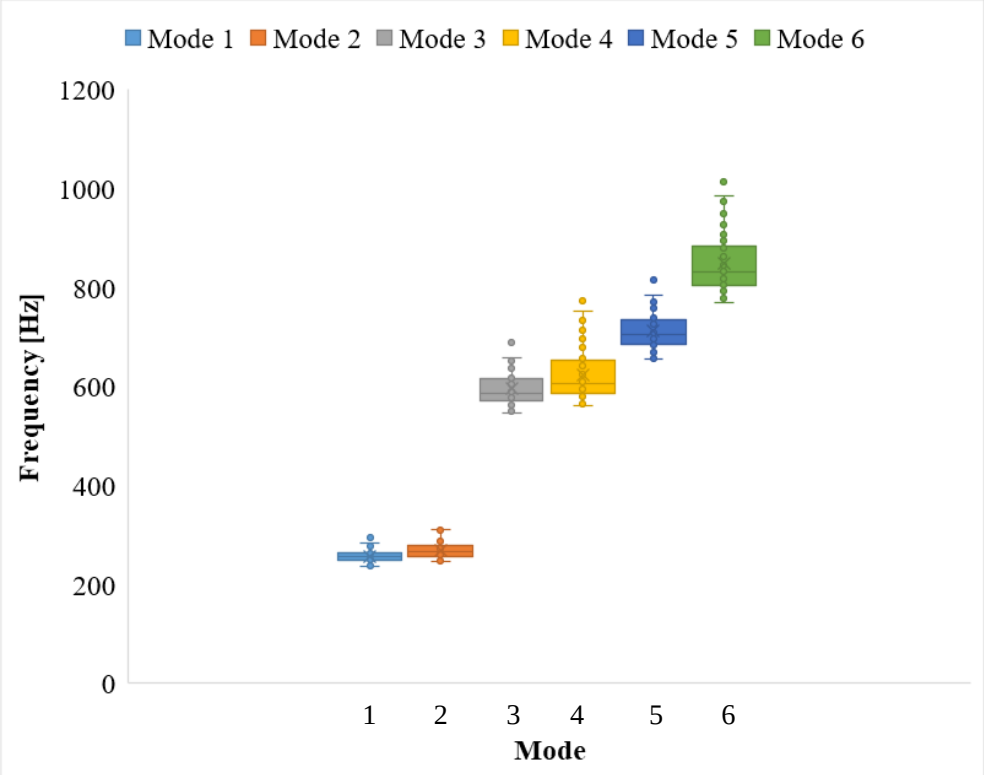

Figure 16. Expected Improvement (EI) evolution for GFRP-BD properties

Table 6. Maximum and minimum limits for the natural frequencies of the GFRP-BD plates

Frequency	$f(1)$	$f(2)$	$f(3)$	$f(4)$	$f(5)$	$f(6)$
Minimum	183.551	191.118	413.854	431.287	495.561	596.674
Maximum	214.525	235.476	524.414	530.396	589.658	730.097
Normalized minimum	0.000	0.001	0.050	0.000	0.000	0.027
Normalized maximum	0.938	1.000	1.000	1.000	1.000	1.000

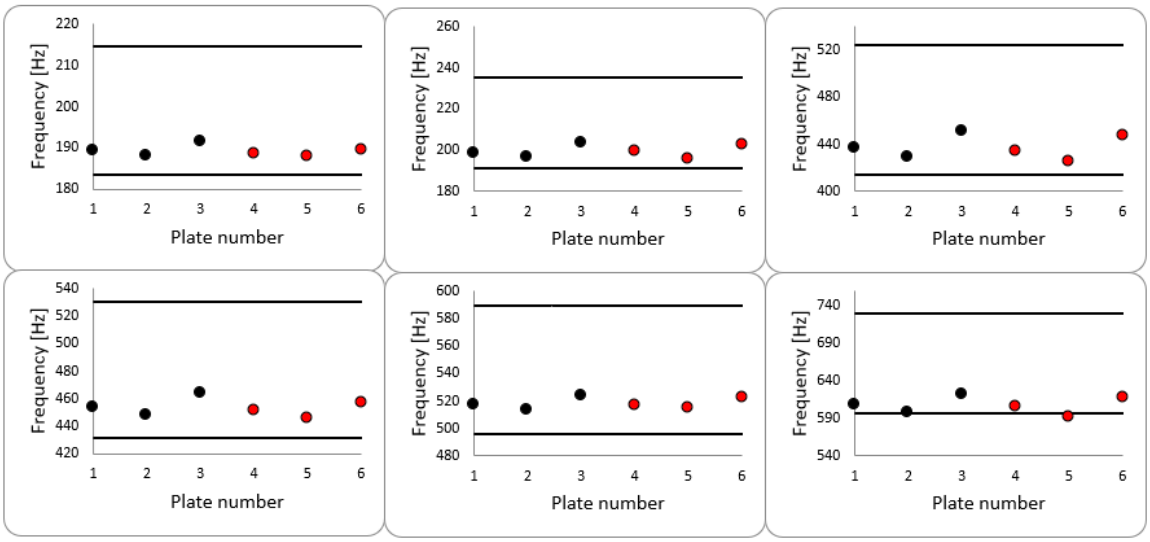

Figure 17. Natural frequency limits and experimental results, intact (black) and damaged (red), for the GFRP-BD plates

It was found that all intact and damaged samples were inside the limits established by the range. By this analysis, all intact samples would not have manufacturing defects. It was observed that intact and damaged samples had similar values for their frequencies.

After analysing the frequency range, the FRFs were obtained using *Abaqus*®. Figure 18 shows the envelope for intact plates created from these points, together with the FRFs from the 6 previously analysed plates. For this envelope, it was considered the data obtained from the accelerometer at point 2 and hammer impact at point 1 shown in the plate.

The FRFs of intact plates were found to be inside the design envelope. Based on the procedure used, this shows the presence of less issues in terms of manufacturing process comparing to UD samples. In fact, this makes sense, because it is easier to stack BD plies instead UD plies, mainly, when it is used hand-lay-up process. In other words, it is easier to guarantee the orientations of the plies specified in the initial design. When analysing the intact and damaged FRFs, considerable differences were observed between the frequencies of 450 and 650 Hz, thus characterizing that plates 4 to 6 had some type of damage. The envelope for the data obtained from the accelerometer at point 3 and the hammer impact at point 1 was also plotted. Figure 19 shows the FRFs envelope for the intact sample created from these points, together with the FRFs of the 6 analysed plates. For this study, it is possible to verify that the intact plates and the damaged plates present divergences in their amplitudes from the frequency value of 350Hz.

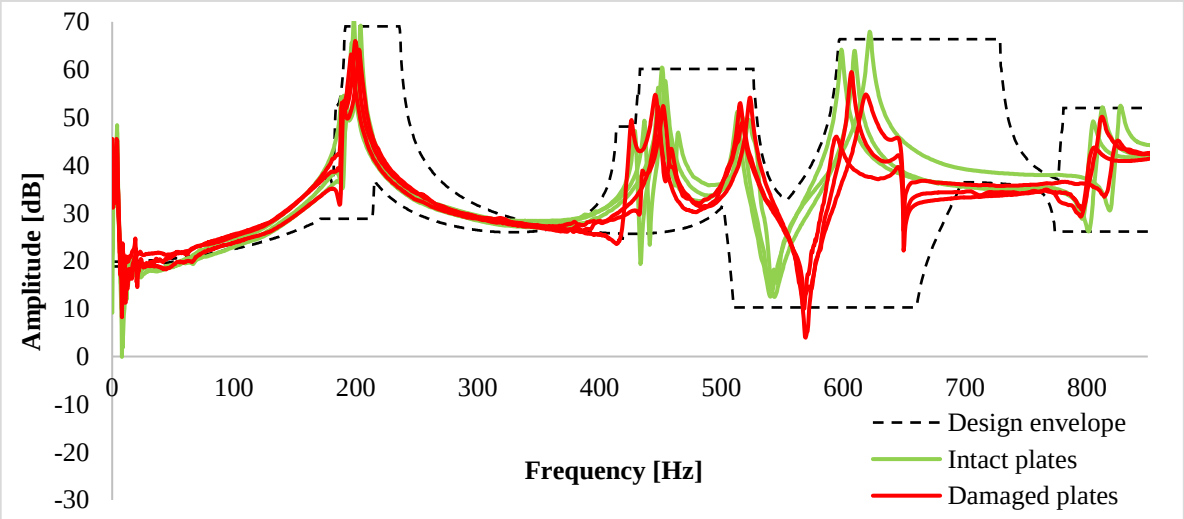

Figure 18. FRFs (H_{21}) envelopes for GFRP-BD plates

Finally, an analysis of the damage indices was carried out. Table 7 presents the damage indices found for the 3 boards analysed. It can be verified that the damage indices presented

high values for both cases, some being more expressive for the data analysed through accelerometer 3, and others from accelerometer 2. With this, it can be confirmed that both samples present impact damage in their structure.

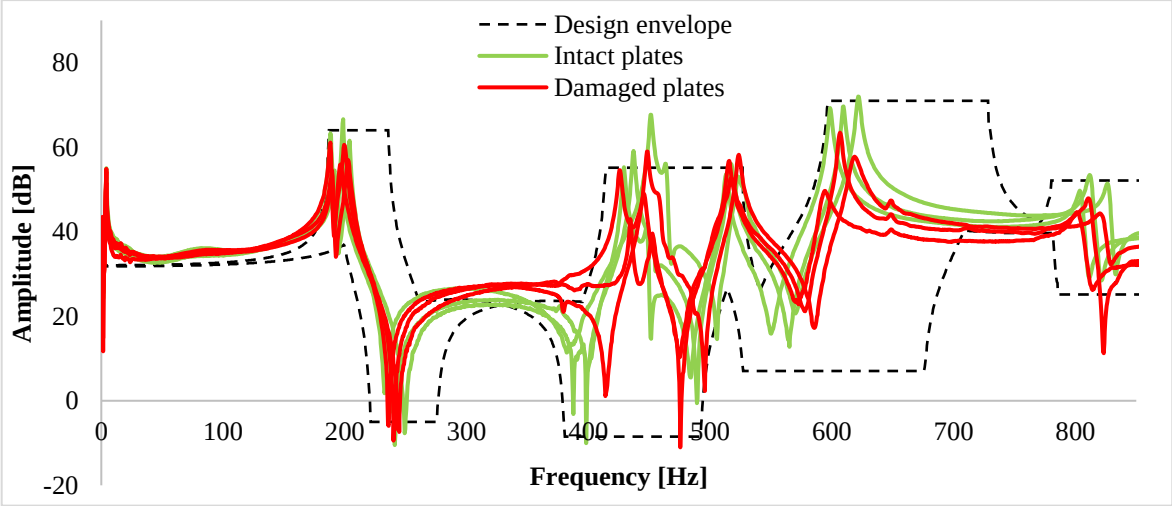

Figure 19. FRFs (H_{31}) envelopes for GFRP-BD plates

Table 7. Damage indices obtained for GFRP-BD plates

Frequency interval analyzed: 0 a 1024 Hz				
Plate	**H_{21}**	**H_{31}**	**Mean**	**Standard deviation**
1	0.609	0.267	0.438	0.171
2	2.578	0.778	1.678	0.900
3	0.730	0.454	0.592	0.138

12. Conclusions

The authors introduce a numerical-experimental procedure to detect defects and impact damage in composite structures. For the application of the proposed procedure, GFRP composite plates made from uni-directional and bi-directional fabrics are used as case studies. Analysis of the properties of the plates is conducted to be used in the Latin Hypercube method. Natural frequencies are obtained from finite element analysis to feed the LH discretization. These inputs and outputs are the basis for the construction of the Kriging metamodel. 31 more data points are added to complement the Kriging database using the EGO technique. Finally, numerical runs with the highest and lowest frequencies are selected to generate the natural frequency envelopes and the FRFs envelopes. Therefore, the envelopes can be used to select better composite structures in terms of manufacturing quality.

Considering the UD GFRP composite samples, it was verified that all samples are in the lower limit, and may have manufacturing defects. This information was confirmed through the

design envelope. By analysing frequencies and comparing the FRFs of intact and damaged samples, no information on damage can be obtained. It was possible to verify the damage only through the damage indices. When analysing the group of BD GFRP composite samples, it was verified through the frequencies and the design envelope that all intact samples present less manufacturing issues than UD samples, which are more complicated to have the plyes stacked acoording to the design specifications. When analysing the FRFs of intact damaged samples, no damage information could be obtained. However, based on the damage index, it can be seen that the samples had some type of damage.

Finally, it was possible to verify the influence of adding metrics to the Latin Hypercube, collaborating in the development of the metamodel, reducing the computational cost, and consequently providing a gain in time at the end of the simulation. An approximated function is obtained to generate the design envelope to analyse the manufacturing process of the structure. Te proposed procedure is a kind of inspection tool to quantify the quality of composite structures. In fact, through this tool, considering the limits imposed in the initial design, it is possible to quickly inspect post-manufactured composite structures by using a vibration-based method. Therefore, the present work contributes to the development of a non-destructive inspection method by applying a proposed procedure based on experimental and numerical analysis. In addition, the proposed procedure can provide the foundations for the next generation of systems for detecting defects from the manufacturing process of real composite structures, as well as damage indices for damages caused during the life of the structure. Therefore, the present work is one more contribution to a methodology proposed by the authors over the years [17-18, 33-38]. Thus, the methodology, which incorporates a new damage metric combined to shearography speckle technique and flexure after impact to detect, locate, and mainly, to provide information on the extent of damage and the residual strength in composite structures, can include the proposed procedure to evaluate the influence of manufacturing process on the dynamic behavior of the composite structures, as well. In other words, the authors have improved their methodology in order to be used in advanced SHM systems for composite structures.

Acknowledgments

The authors acknowledge the financial support of the Santa Catarina State Research and Innovation Foundation (FAPESC number: 2017TR1747, 2019TR779, 2021TR843, and 2023TR563). As well as, Sao Paulo State Research Foundation (FAPESP number: 2012/01047-

8 and 2015/15221-8), Coordination for the Improvement of Higher Level Personnel (CAPES number: 011214/2013-09 and Finance Code 001), PROMOP (Programa de Bolsas de Monitoria de Pós-Graduação) of the Santa Catarina State University. Ricardo De Medeiros acknowledges the financial support of the National Council for Scientific and Technological Development (CNPq process number: 304795/2022-4). Volnei Tita acknowledges the financial support of the National Council for Scientific and Technological Development (CNPq number: 310159/2022-9).

Competing interest

No potential competing interest was reported by the authors.

References

[1] HESLEHURST RB. *Defects and damage in composite materials and structures*. CRC Press, Boca Raton, Florida, United States, 2014.

[2] WIEGAND J, HORNIG A, GERLACH R, NEALE C, PETRINIC N, HUFENBACH W. An experimental method for dynamic delamination analysis of composite materials by impact bending. *Mechanics of Advanced Materials and Structures*, v. 22, p. 413-21, 2015. (https://doi.org/10.1080/15376494.2012.736066)

[3] CAMPBELL FC. *Structural composite materials*. ASM International, Ohio, United States, 2010.

[4] SHEN FC. A filament-wound structure technology overview. *Materials Chemistry and Physics*, v. 42, p. 96-100, 1995. (https://doi.org/10.1016/0254-0584(95)01554-X)

[5] CALLISTER WD, RETHWISCH DG. *Materials science, and engineering: an introduction*. John Wiley & sons, New York, NY, 2007.

[6] DOHERTY JE. *Nondestructive Evaluation*, Chapter 12 in Handbook on Experimental Mechanics, AS Kobayashi Edt. Society for Experimental Mechanics, Inc., 1987.

[7] ZHANG, G., TANG, L., LIU, Z., ZHOU, L., LIU, Y. AND JIANG, Z. Machine-learning-based damage identification methods with features derived from moving principal component analysis. *Mechanics of Advanced Materials and Structures*, v. 27, n. 21, p. 1789-1802, 2020. (https://doi.org/10.1080/15376494.2019.1710308)

[8] SRIRAMULA S, CHRYSSANTHOPOULOS MK. Quantification of uncertainty modelling in stochastic analysis of FRP composites. *Composites Part A: Applied Science and Manufacturing*, v. 40, p. 1673-1684, 2009. (https://doi.org/10.1016/j.compositesa.2009.08.020)

[9] QIAO, L., YAN, W. AND CAO, S. Inverse analysis for damage detection in a rod using EMI method. *Mechanics of Advanced Materials and Structures*, v. 30, n. 1, p. 168-174, 2023. (https://doi.org/10.1080/15376494.2021.2010845)

[10] HOUSNER GW, BERGMAN LA, CAUGHEY TK, CHASSIAKOS AG, CLAUS RO, MASRI SF, SKELTON RE, SOONG TT, SPENCER BF, JAMES JTP. Structural control: past, present, and future. *Journal of engineering mechanics*, v. 123, n. 9, p. 897-971, 1997. (https://doi.org/10.1061/(ASCE)0733-9399(1997)123:9(897))

[11] SINOU JJ. A review of damage detection and health monitoring of mechanical systems from changes in the measurement of linear and non-linear vibrations. *Mechanical Vibrations: Measurement, Effects and Control*, p.643-702, 2009. (https://hal.science/hal-00779322)

[12] OLIVER, G.A., PEREIRA, J.L.J., FRANCISCO, M.B. AND GOMES, G.F. The influence of delamination parameters on the wavelet based damage index in CFRP structures. *Mechanics of Advanced Materials and Structures*, v. 30, n. 6, p. 1117-1127, 2023. (https://doi.org/10.1080/15376494.2022.2028204)

[13] MONTALVAO D, MAIA NMM, RIBEIRO AMR. A Review of Vibration-based Structural Health Monitoring with Special Emphasis on Composite Materials. *The Shock and Vibration Digest*, v. 38, p. 295-324, 2006. (https://doi:10.1177/0583102406065898)

[14] FARRAR CR, DOEBLING SW, NIX DA. Vibration-based structural damage identification. *Philosophical Transactions of the Royal Society of London. Series A: Mathematical, Physical and Engineering Sciences*, v. 359, n. 1778, p. 131-149, 2001. (https://doi.org/10.1098/rsta.2000.0717)

[15] KESSLER SS, MARK SPEARING S, ATALLA MJ, CESNIK CES, SOUTIS C. Damage detection in composite materials using frequency response methods. *Composites Part B: Engineering*, v. 33, n. 1, p. 87-95, 2002. (https://doi.org/10.1016/S1359-8368(01)00050-6)

[16] SANTOS, J.V., SOARES, C.M., SOARES, C.A. AND PINA, H.L.G. Identification of damage in composite structures: a numerical model. *Mechanics of Composite Materials and Structures*, v. 6, n. 4, p. 363-376, 1999. (https://www.tandfonline.com/doi/abs/10.1080/107594199305511)

[17] DE MEDEIROS R, LOPES HM, GUEDES RM, VAZ MA, VANDEPITTE D, TITA V. A new methodology for Structural Health Monitoring applications. *Procedia Engineering*, v. 114, p. 54-61, 2015. (https://doi.org/10.1016/j.proeng.2015.08.036)

[18] DE MEDEIROS R, VANDEPITTE D, TITA V. Structural health monitoring for impact damaged composite: a new methodology based on a combination of techniques. *Structural Health Monitoring - An International Journal*, v. 17, p. 185-200, 2018. (https://doi.org/10.1177/1475921716688442)

[19] ZHAN, P., QIN, X., ZHANG, Q. AND SUN, Y. Damage identification in beam-like structure using strain FRF-based damage index and artificial neural network. *Mechanics of Advanced Materials and Structures*, v. 30, n. 12, p. 2458-2476, 2023. (https://doi.org/10.1080/15376494.2022.2055241)

[20] JANSSON N, WAKEMAN WD, MÅNSON JA. Optimization of hybrid thermoplastic composite structures using surrogate models and genetic algorithms. *Composite Structures*, v. 80, p. 21-31, 2007. (https://doi.org/10.1016/j.compstruct.2006.02.036)

[21] FORRESTER, A., SOBESTER, A. & KEANE, A. *Engineering design via surrogate modelling: a practical guide*, John Wiley & Sons, Southern Gate, Chichester, West Sussex, United Kingdom, 2008.

[22] JEONG S, MURAYAMA M, YAMAMOTO K. Efficient optimization design method using kriging model. *Journal of aircraft*, v. 42, p. 413-420, 2005. (https://doi.org/10.2514/1.6386)

[23] KLEIJNEN JPC. Kriging metamodeling in simulation: A review. *European Journal of Operational Research*, v. 192, p. 707-716, 2009. (https://doi.org/10.1016/j.ejor.2007.10.013)

[24] ECHAABI J, TROCHU F, GAUVIN R. Review of failure criteria of fibrous composite materials. *Polymer composites*, v. 17, p. 786-798, 1996. (https://doi.org/10.1002/pc.10671)

[25] LANZI L, GIAVOTTO V. Post-buckling optimization of composite stiffened panels: Computations and experiments. *Composite Structures*, v. 73, p. 208-220, 2006. (https://doi.org/10.1016/j.compstruct.2005.11.047)

[26] LU J, ZHU P, JI Q, FENG Q, HE J. Identification of the mechanical properties of the carbon fiber and the interphase region based on computational micromechanics and Kriging metamodel. *Computational Materials Science*, v. 95, p. 172-180, 2014. (https://doi.org/10.1016/j.commatsci.2014.07.034)

[27] MUKHOPADHYAY T, CHAKRABORTY S, DEY S, ADHIKARI S, CHOWDHURY R. A critical assessment of Kriging model variants for high-fidelity uncertainty quantification in dynamics of composite shells. *Archives of Computational Methods in Engineering*, v. 24, p. 495-518, 2017. (https://doi.org/10.1007/s11831-016-9178-z)

[28] PAVLACK B, PAIXÃO J, DA SILVA S, CUNHA A, CAVA DG. Polynomial Chaos-Kriging metamodel for quantification of the debonding area in large wind turbine blades. *Structural Health Monitoring*, v. 21, n. 2, p. 666-682, 2021. (https://doi.org/10.1177/14759217211007956)

[29] MUKHOPADHYAY T. A multivariate adaptive regression splines based damage identification methodology for web core composite bridges including the effect of noise. *Journal of Sandwich Structures & Materials*, v. 20, n. 7, p. 885-903, 2018. (https://doi.org/10.1177/1099636216682533)

[30] LIU B, VU-BAC N, ZHUANG X, FU X, RABCZUK T. Stochastic integrated machine learning based multiscale approach for the prediction of the thermal conductivity in carbon nanotube reinforced polymeric composites. *Composites Science and Technology*, v. 224, p. 109425, 2022. (https://doi.org/10.1016/j.compscitech.2022.109425)

[31] RIKARDS R., ABRAMOVICH H, GREEN T, AUZINS J., CHATE A. Identification of elastic properties of composite laminates. *Mechanics of Advanced Materials and Structures*, v. 10, n. 4, p.335-352, 2003. (https://doi.org/10.1080/10759410306755)

[32] GHASEMI FA, NIYARAKI MN, GHASEMI I, DANESHPAYEH S. Predicting the tensile strength and elongation at break of PP/graphene/glass fiber/EPDM nanocomposites using response surface methodology. *Mechanics of Advanced Materials and Structures*, v. 28, n. 10, p. 981-989, 2021. (https://doi.org/10.1080/15376494.2019.1614702)

[33] DE MEDEIROS R, RODRÍGUEZ-RAMOS R, GUINOVART-DÍAZ R, BRAVO-CASTILLERO J, OTERO JÁ, TITA V. Numerical and analytical analyses for active fiber composite piezoelectric composite materials. *Journal of Intelligent Material Systems and Structures*, v. 26, n. 1, p. 101-118, 2015. (https://doi.org/10.1177/1045389X14521881)

[34] SARTORATO M, DE MEDEIROS R, TITA V. A finite element formulation for smart piezoelectric composite shells: Mathematical formulation, computational analysis and experimental evaluation. *Composite Structures*, v. 127, p. 185-198, 2015. (https://doi.org/10.1016/j.compstruct.2015.03.009)

[35] DE MEDEIROS R, SARTORATO M, VANDEPITTE D, TITA V. A comparative assessment of different frequency based damage detection in unidirectional composite plates using MFC sensors. *Journal of Sound and Vibration*, v. 383, p.171-190, 2016. (https://doi.org/10.1016/j.jsv.2016.06.047)

[36] SARTORATO M, DE MEDEIROS R, VANDEPITTE D, TITA V. Computational model for supporting SHM systems design: Damage identification via numerical analyses. *Mechanical Systems and Signal Processing*, v. 84, p. 445-461, 2017. (https://doi.org/10.1016/j.ymssp.2016.07.035)

[37] MARQUES D, FLOR FR, MEDEIROS RD, PAGANI JUNIOR CDC, TITA V. Structural health monitoring of sandwich structures based on dynamic analysis. *Latin American Journal of Solids and Structures*, v. 15, p. 58, 2018. (https://doi.org/10.1590/1679-78254309)

[38] DOS SANTOS SOUZA LF, VANDEPITTE D, TITA V, DE MEDEIROS R. Dynamic response of laminated composites using design of experiments: An experimental and numerical study. *Mechanical Systems and Signal Processing*, v. 115, p. 82-101, 2019. (https://doi.org/10.1016/j.ymssp.2018.05.022)

[39] HOYLE N. Automated multi-stage geometry parameterization of internal fluid applications. *Ph.D. Thesis*, University of Southampton, 2006.

[40] FANG J, SUN G, QIU N, KIM NH, LI Q. On design optimization for structural crashworthiness and its state of the art. *Structural and Multidisciplinary Optimization*, v. 55, n. 3, p. 1091-1119, 2017. (https://doi.org/10.1007/s00158-016-1579-y)

[41] VIANA FA. A tutorial on latin hypercube design of experiments. *Quality and Reliability Engineering International*, v. 32, n. 5, p. 1975-1985, 2016. (https://doi.org/10.1002/qre.1924)

[42] JOHNSON ME, MOORE LM, YLVISAKER D. Minimax and maximin distance designs. *Journal of statistical planning and inference*, v. 26, n. 2, p. 131-148, 1990. (https://doi.org/10.1016/0378-3758(90)90122-B)

[43] MORRIS MD, MITCHELL TJ. Exploratory designs for computational experiments. *Journal of statistical planning and inference*, v. 43, n. 3, p. 381-402, 1995. (https://doi.org/10.1016/0378-3758(94)00035-T)

[44] SIMPSON TW, POPLINSKI JD, KOCH PN, ALLEN JK. Metamodels for computer-based engineering design: survey and recommendations. *Engineering with Computers*, v. 17, p. 129-150. (https://doi.org/10.1007/PL00007198)

[45] MARTIN JD, SIMPSON TW. Use of kriging models to approximate deterministic computer models. *AIAA Journal*, v. 43, n. 4, p. 853-863, 2005. (https://doi.org/10.2514/1.8650)

[46] JONES DR, SCHONLAU M, WELCH WJ. Efficient Global Optimization of Expensive Black-Box Functions. *Journal of Global Optimization*, v. 13, n. 4, p. 455-492, 1998. (https://doi.org/10.1023/A:1008306431147)

[47] FERREIRA WG. *Efficient Global Optimization driven by ensemble of metamodels: new directions opened by least squares approximation*, report, 2016.

[48] EMMERICH M, KLINKENBERG J. *The computation of the expected improvement in dominated hypervolume of Pareto front approximations*. Rapport technique, Leiden University, v. 34, p. 7 3, 2008.

[49] SCHONLAU M. *Computer experiments and global optimization*. Ph.D. thesis, Statistics, University of Waterloo, Waterloo, Ontario, Canada, 1997.

[50] DE MEDEIROS R. Development of a criterion for predicting residual strength of composite structures damaged by impact loading. *Ph.D. Thesis*, São Carlos School of Engineering, University of São Paulo, São Carlos, Brazil, 2016. (https://www.teses.usp.br/teses/disponiveis/18/18148/tde-26072016-221608/en.php)

[51] DA COSTA RR, SATO ES, RIBEIRO ML, DE MEDEIROS R, VIEIRA AF, GUEDES RM, TITA V. Polyurethane derived from castor oil reinforced with long cotton fibers: Static and dynamic testing of a novel eco-friendly composite material. *Journal of Composite Materials*, v. 54, n. 22, p.3125-3142, 2020. (https://doi.org/10.1177/0021998320911984)

[52] SILVA HP. Comportamento mecânico de compósitos de fibra de vidro/epoxy nano-reforçados, *Tese de doutoramento*. p. 240. Universidade de Coimbra, Coimbra, 2014. (http://hdl.handle.net/10316/28115)

[53] SINGH KK, SINGH NK, JHA R. Analysis of symmetric and asymmetric glass fiber reinforced plastic laminates subjected to low-velocity impact. *Journal of Composite Materials*, v. 50, n. 14, p.1853-1863, 2016. (https://doi.org/10.1177/0021998315596594)

[54] SUTCLIFFE MPF, LEMANSKI SL, SCOTT A. Measurement of fibre waviness in industrial composite components. *Composites Science and Technology*, v. 72, n. 16, p. 2016-2023, 2012. (https://doi.org/10.1016/j.compscitech.2012.09.001)

[55] ABRATE S. Impact on laminated composites: recent advances. *Applied Mechanics Reviews*, v. 47, n. 11, p. 517-544, 1994. (https://doi.org/10.1115/1.3111065)

[56] DAVIES GAO, ZHANG X. Impact damage prediction in carbon composite structures. *International Journal of Impact Engineering*, v. 16, n. 1, p. 149-170, 1995. (https://doi.org/10.1016/0734-743X(94)00039-Y)

[57] OLSSON R. Analytical prediction of large mass impact damage in composite laminates. *Composites Part A: Applied Science and Manufacturing*, v. 32, n. 9, p. 1207-1215, 2001. (https://doi.org/10.1016/S1359-835X(01)00073-2)

[58] ROBINSON P, DAVIES GAO. Impactor mass and specimen geometry effects in low velocity impact of laminated composites. *International Journal of Impact Engineering*, v. 12, n. 2, p. 189-207, 1992. (https://doi.org/10.1016/0734-743X(92)90408-L)

[59] ZHANG C, ZHENG X, ZHU K, PENG J, WANG Z, LAN L. Experimental investigation of low-velocity impact behavior and CAI on composite laminates by discrete interleaved toughening. *Mechanics of Advanced Materials and Structures*, v. 13, p. 1-2, 2022. (https://doi.org/10.1080/15376494.2022.2158504)

[60] ASTM D7136/D7136M-05:2015. Standard Test Method for Measuring the Damage Resistance of a Fiber-Reinforced Polymer Matrix Composite to a Drop-Weight Impact Event, ASTM International: West Conshohocken, 2015.

[61] ABAQUS, *Documentation*. Pawtucket: Hibbitt, Karlsson & Sorensen, 2021.

[62] XIAO N-C, YUAN K, ZHOU C. Adaptive kriging-based efficient reliability method for structural systems with multiple failure modes and mixed variables. *Computer Methods in Applied Mechanics and Engineering*, v. 359, p. 112649, 2020. (https://doi.org/10.1016/j.cma.2019.112649)

[63] DAMMAK K, BAKLOUTI A, EL HAMI A. Optimal reliable design of brake disk using a Kriging surrogate model. *Mechanics of Advanced Materials and Structures*, v. 29, n. 28, p. 7569-78, 2022. (https://doi.org/10.1080/15376494.2021.2002983)

[64] PALAR PS, SHIMOYAMA K. On efficient global optimization via universal Kriging surrogate models. *Structural and Multidisciplinary Optimization*. v. 57, p. 2377-97, 2018. (https://doi.org/10.1007/s00158-017-1867-1)

[65] KLEIJNEN JP, VAN BEERS W, VAN NIEUWENHUYSE I. Expected improvement in efficient global optimization through bootstrapped kriging. *Journal of global optimization*. v. 54, p. 59-73, 2012. (https://doi.org/10.1007/s10898-011-9741-y)